eLife

Reviewed Preprint
v1 • July 10, 2026
Not revised

For correspondence:
jianghaolouisliu@gmail.com

† shared senior authorship

Competing interests: No competing interests declared

Funding: See page 22

Reviewing editor: Roberto Bottini, University of Trento, Italy

Congenital aphantasia reveals frontotemporal and cingulate structural alterations underlying conscious access to imagery

Yusaku Takamura[1,2], Romain Delsanti[1,3], Laurent Cohen[1], Paolo Bartolomeo[1,†], Jianghao Liu[1,4,†]

[1]Sorbonne Université, Institut du Cerveau - Paris Brain Institute - ICM, Inserm, CNRS, AP-HP, Hôpital de la Pitié-Salpêtrière, Paris, France • [2]Neurorehabilitation Research Center, Kio University, Nara, Japan • [3]Cyceron, Caen Normandie University, GIP Cyceron, Campus Jules Horowitz, Caen, France • [4]Corporate Research, Dassault Systèmes, Vélizy-Villacoublay, France

eLife Assessment

This **valuable** study provides novel evidence that congenital aphantasia is associated with structural differences in frontotemporal and cingulate systems, with relative sparing of early visual regions and major visual pathways. The multimodal structural imaging approach is carefully implemented and will be of interest to researchers studying mental imagery and aphantasia. However, the strength of evidence is **incomplete** because the data cannot adjudicate between alternative cognitive interpretations, and the multiple discovery streams make the findings better viewed as key exploratory evidence, rather than as establishing a definitive structural phenotype of aphantasia.

https://doi.org/10.7554/eLife.111728.1.sa4

Abstract

Congenital aphantasia is characterized by a lifelong absence of voluntary visual imagery despite preserved visual knowledge, offering a natural model for dissociating sensory representation from conscious imagery. Functional imaging evidence suggests that this dissociation may arise from altered top-down interactions between higher-order control systems and high-level visual cortex, but its structural correlates remain unknown. Here, using diffusion and structural MRI in 18 individuals with congenital aphantasia and 18 matched visualisers, we tested two competing accounts of aphantasia: one predicting structural differences in visual pathways, the other predicting differences in higher-order associative networks. Across complementary analyses of white-matter tract microstructure, functional-ROI tractography, graph-theoretic network organization, and cortical morphometry, aphantasia was associated with selective structural differences in frontotemporal and cingulate white-matter tracts — including the uncinate fasciculus, posterior interparietal callosal fibers, and dorsal cingulum — and in frontotemporal cortical regions, including the anterior insula, anterior prefrontal cortex, and medial temporal cortex. By contrast, we found no reliable group differences in early visual cortex, major visual tracts, or the direct structural connections of the core imagery network. Congenital aphantasia therefore exhibits a selective structural phenotype centered on frontotemporal and cingulate systems, sparing the principal visual pathways. These findings suggest that higher-order systems supporting integration and conscious access — rather than visual representations themselves — constitute the primary structural substrate of absent conscious imagery in congenital aphantasia.

Introduction

Congenital aphantasia, characterized by a lifelong absence of voluntary visual mental imagery, affects an estimated 2–4% of the population (Zeman, 2024) and presents a striking paradox (Liu & Bartolomeo, 2025; Arcangeli & Bartolomeo, 2025): aphantasic individuals can accurately retrieve visual properties of objects from memory and perform normally on many visual imagery tasks, yet report little or no subjective imagery experience (Siena & Simons, 2024; Liu & Bartolomeo, 2023; Pounder et al., 2022; Suggate et al., 2026). This dissociation suggests that access to visual knowledge can be preserved even when the phenomenological experience of imagery is absent (Liu & Bartolomeo, 2023). Congenital aphantasia therefore provides a useful model for understanding what higher-order mechanisms are necessary to transform internally generated representations into conscious imagery experience (Liu, 2026, in press).

Beyond the absence of visual imagery, congenital aphantasia has been associated with a broader cognitive and affective profile consistent with a neurodevelopmental condition (Sokolowski & Levine, 2023). Aphantasic individuals retrieve fewer phenomenological details from autobiographical events and show reduced hippocampal-occipital functional connectivity during memory recall (Zeman et al., 2020; Dawes et al., 2022; Monzel et al., 2024b). Difficulties in domains such as face recognition and emotional awareness have also been reported (Dance et al., 2023; Monzel et al., 2024a; Zeman et al., 2020) and intrusive memories are less likely to take a visual form in aphantasics (Keogh et al., 2023). Together with the suggested co-occurrence of aphantasia with neurodevelopmental conditions primarily affecting higher-order rather than sensory systems (Dance et al., 2021; Milton et al., 2021; Mawtus et al., 2024), these findings suggest that aphantasia may involve higher-order systems extending beyond visual representation alone. Whether this broader profile is associated with a common structural substrate remains unknown.

Structural neuroimaging offers one way to test whether the functional alterations reported in aphantasia have an anatomical basis. In neurodevelopmental conditions, functional alterations often co-occur with white-matter microstructural differences, suggesting that atypical connectivity may arise from altered axonal development rather than acquired disruption — as seen for example in congenital prosopagnosia, ADHD, and autism spectrum conditions (Parlatini et al., 2023; Thomas et al., 2009; Travers et al., 2012). The suggested association of congenital aphantasia with some of these conditions, together with reports of altered autobiographical memory, face recognition, and emotional awareness (Zeman et al., 2020; Dawes et al., 2022; Dance et al., 2023; Monzel et al., 2024a), raises the possibility that aphantasia is associated with structural differences in fronto-temporal and cingulate systems. Characterizing these structural correlates may therefore illuminate both the stability of the condition across the lifespan and its broader cognitive profile (Liu, 2026; Zeman et al., 2020).

Neuroimaging studies of aphantasia (Milton et al., 2021; Liu et al., 2025a; Chang et al., 2025; Liu et al., 2025b; Cabbai et al., 2024; Montabes De La Cruz et al., 2024) have yielded two competing accounts. One view holds that aphantasia arises from alterations in visual pathways or early visual cortex, reflecting reduced sensory strength of internally generated representations (Keogh & Pearson, 2018). Consistent with this possibility, aphantasic individuals show altered decoding during imagery in V1, suggesting that imagery representations may not reach the perceptual-like format typically associated with vivid imagery experience (Chang et al., 2025). An alternative account emphasizes disrupted top-down modulation from higher-order brain regions (Liu, 2026; Liu & Bartolomeo, 2025). During imagery tasks, despite preserved activity in high-level visual areas, aphantasic individuals show reduced functional coupling between the fusiform imagery node (FIN)—a region of fusiform cortex selectively activated during visual imagery (Bartolomeo et al., 2026; Liu et al., 2025b; Spagna et al., 2021)—and left prefrontal regions (Liu et al., 2025b), including the anterior prefrontal cortex (aPFC) and frontal eye field (FEF). Higher-order attention and salience regions, including FEF and anterior insula, have been proposed to contribute to the top-down amplification of internally generated representations and their segregation from external input (Corbetta & Shulman, 2002). This view is further

supported by reduced representational overlap between imagery and perception in high-level visual regions (Liu et al., 2025b) and orbitofrontal cortex (OFC; Liu et al., 2025a), as well as altered frontoparietal-temporal coupling and reduced neural signal complexity (Noble et al., 2026). These accounts make different structural predictions: a local visual-pathway account predicts differences in posterior visual tracts, including the vertical occipital fasciculus (VOF), inferior longitudinal fasciculus (ILF), and inferior fronto-occipital fasciculus (IFOF), whereas a higher-order account predicts differences in fronto-temporal and cingulate pathways.

Here, we tested these competing predictions using diffusion-weighted and T1-weighted MRI. We combined four complementary approaches—tractometry, functional region-of-interest (fROI)-based tractography, graph-theoretic network analysis, and surface-based cortical morphometry—to characterize potential group differences across tract, network, and cortical scales (see analysis pipeline in Fig. S1).

Results

Atlas-based tractometry reveals selective microstructural differences

We quantified fractional anisotropy (FA) along atlas-defined major white-matter tracts, providing a tract-profile measure of white-matter microstructure. We assessed major tracts associated with visual processing, including the VOF, IFOF, and ILF, as well as tracts associated with higher-order functions, including fronto-parietal attention pathways (Superior longitudinal fasciculus: SLFs, Arcuate fasciculus: AF), medial fronto-temporal pathways (Uncinate fasciculus: UF, ventral cingulum), and cognitive-control pathways (dorsal cingulum).

Figure 1 and Table S1 show the tractometry results. No significant FA differences were detected in the visual tracts examined. In contrast, group differences were observed in several higher-order associative pathways. Relative to visualizers, aphantasic individuals showed reduced FA in both the left and right UF, localized to the anterior temporal segment (Fig. 1A). Reduced FA was also observed in the posterior interparietal corpus callosum. By contrast, aphantasic individuals showed increased FA across much of the bilateral dorsal cingulum (Fig. 1B). No significant clusters were identified in the remaining tracts.

To further characterize these findings, we examined axial diffusivity (AD), radial diffusivity (RD), and neurite orientation dispersion and density imaging (NODDI) metrics at the affected segments (Fig. S2 and Table S1). These follow-up analyses were consistent with microstructural differences rather than fiber geometry alone, such as crossing-fiber artefact.

The right SLF-II and right ventral cingulum showed marginal reductions in FA (Fig. S3); however, these effects may be confounded by fiber geometry and were therefore not interpreted further.

Graph-theoretic network analysis reveals disrupted segregation and inter-network hubness

We next applied graph-theoretic analysis to examine whether the tract-level differences extended to the structural organization of large-scale brain networks. We generated a 400 × 400 whole-brain structural connectivity matrix based on the Schaefer 17-network parcellation (see analysis pipeline in Fig. 2A). From this weighted undirected graph, we computed node-level metrics to characterize network organization. Given the study hypothesis, analyses focused on nodes within the visual, attention, salience, and default mode networks.

Group differences were observed in three higher-order network metrics (Fig. 2B–D; Table S2). In aphantasia, the left FEF, a key node of the dorsal attention network (DAN B in Fig. 2A), showed reduced node strength, indicating weaker overall structural connectivity at this node. The left anterior insula, part of the salience/ventral attention network (VAN A), and the left dorsolateral prefrontal cortex (dlPFC) of the default mode network (Default B) showed decreased

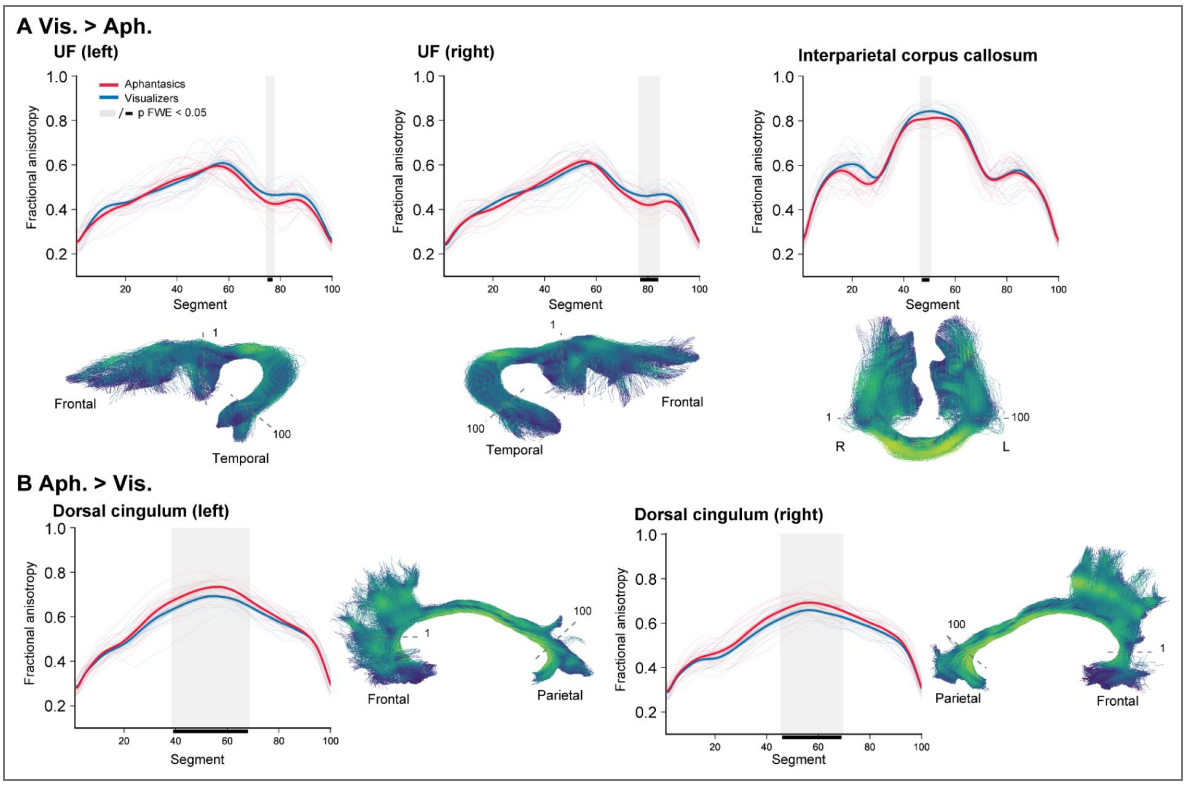

Figure 1. Tractometry reveals selective white-matter microstructural differences in aphantasia.

(A) Tracts showing reduced fractional anisotropy (FA) in aphantasic individuals relative to visualizers (Vis. > Aph.): left uncinate fasciculus (UF), right UF, and posterior interparietal corpus callosum. Upper panels show tract profiles (mean ± SEM); lower panels show tract reconstructions from a representative participant, color-coded by segment position (nodes 1-100). Red lines indicate aphantasic individuals and blue lines indicate visualizers. Shaded gray regions mark segments showing significant group differences ($p < 0.05$, FWE-corrected). **(B)** Tracts showing increased FA in aphantasic individuals relative to visualizers (Aph. > Vis.): left and right dorsal cingulum. Upper panels show tract profiles (mean ± SEM); lower panels show representative tract reconstructions, color-coded by segment position. Red lines indicate aphantasic individuals and blue lines indicate visualizers. Shaded gray regions and black bars on the x axis mark significant segments ($p < 0.05$, FWE-corrected). Thin lines show individual participant profiles; thick lines show group means.

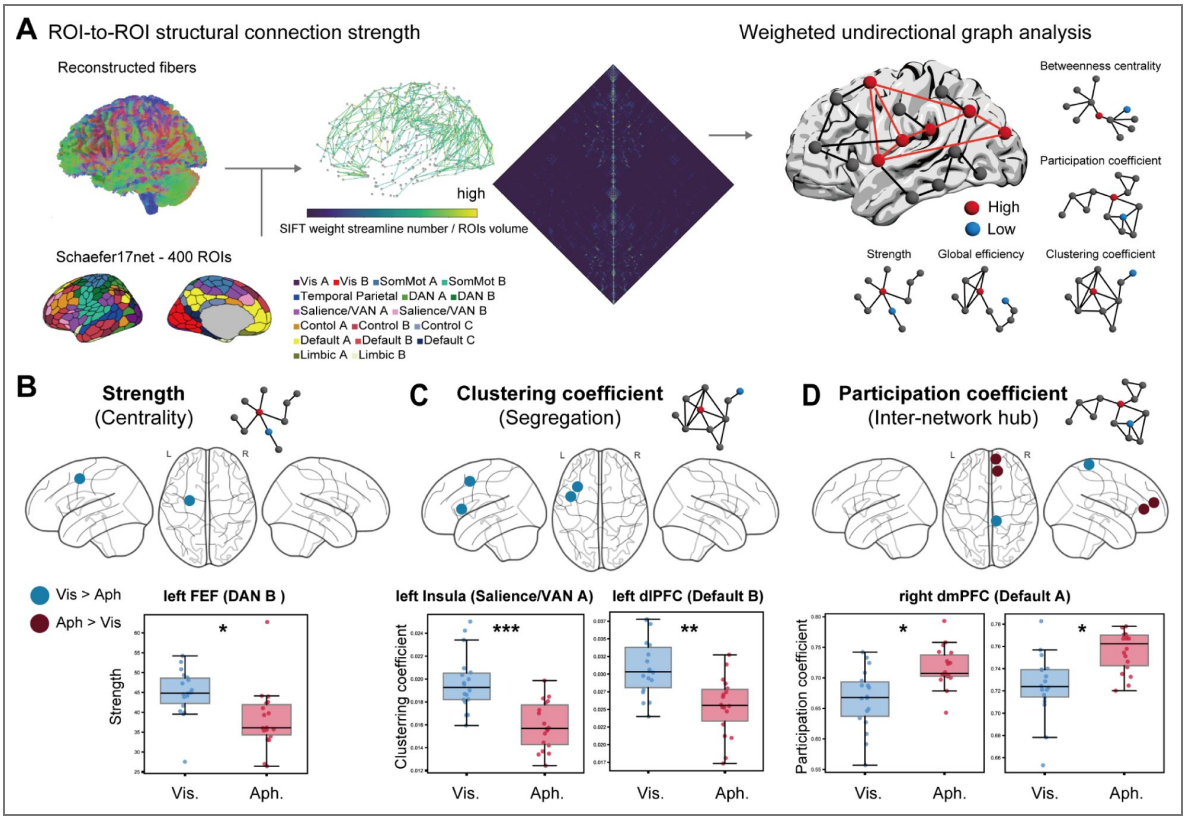

Figure 2. Structural network analysis reveals reduced local segregation and increased inter-network hubness in congenital aphantasia.

(A) Analysis pipeline. Whole-brain tractography streamlines were weighted using spherical-deconvolution informed filtering of tractograms (SIFT2) and normalized by ROI volume to generate a 400 × 400 structural connectivity matrix based on the Schaefer 17-network parcellation. Node-level graph-theoretic metrics were then computed from the weighted undirected graph. **(B)** Node strength was reduced in the left frontal eye field (FEF; dorsal attention network B, DAN B) in aphantasic individuals relative to visualizers, indicating weaker overall structural connectivity at this node. **(C)** Clustering coefficient was reduced in the left anterior insula (salience/ventral attention network A, Sal/VAN A) and left dorsolateral prefrontal cortex (dlPFC; Default B), indicating reduced local network segregation in salience and association-network regions. **(D)** Participation coefficient was increased in the right dorsomedial prefrontal cortex (dmPFC; Default A) in aphantasia, indicating greater inter-network hubness at this node. Blue indicates Vis. > Aph.; dark red indicates Aph. > Vis. Boxplots show median and interquartile range; *p < 0.05, **p < 0.01, ***p < 0.001, FWE-corrected.

clustering coefficient, indicating reduced local network segregation in salience and cognitive-control regions. By contrast, the right dorsomedial prefrontal cortex (dmPFC) of the default mode network (Default A) showed increased participation coefficient, indicating stronger inter-network hubness in aphantasic individuals. In addition, the right somatomotor network showed reduced participation coefficient in aphantasic individuals. Control analyses using alternative parcellations confirmed that these findings were robust across atlas options (Fig. S5A–B).

Tracing direct structural connections to these nodes showed that the left anterior insula was connected primarily via the AF and IFOF (Fig. S5C), whereas dmPFC connectivity involved dorsal cingulum pathways. These anatomical relationships are considered further in the Discussion.

By contrast, no significant differences were observed in the visual cortex nodes examined, in keeping with the absence of tractometry differences in the major visual pathways.

No difference found in white-matter connections of the core imagery network

We next characterized the white-matter connections of a core imagery network whose functional properties are altered in aphantasia. We defined fROIs on the basis of our 7T fMRI results (Liu et al., 2025b): the FIN, left aPFC, left OFC, and right anterior intraparietal sulcus (aIPS). For each of the four ROIs (Fig. S4A) in each group, we identified streamlines intersecting its projection on the grey/white-matter interface and quantified tract structure using two indices: volume-normalized streamline count (Fig. S4B) and streamline proportion (Fig. S4C) within anatomically defined bundles. No significant between-group differences were observed for either index in any tract or ROI after correction for multiple comparisons. Bayes factor (BF) analysis further provided some moderate evidence for the absence of a group difference, thus consistent with an equivalence, in volume-normalized streamline count in the VOF connecting the FIN (BF = 0.32), the major white-matter bundle linking dorsal and ventral visual cortex. Together, these findings indicate no reliable alteration in the direct structural connections examined within the core imagery network.

Cortical thickness: reduced in the left aPFC, increased in limbic regions

We finally examined cortical thickness across the whole brain. Prior work has linked prefrontal and early visual cortical thickness to individual differences in imagery vividness (Bergmann et al., 2016a, 2016b), including a relationship between smaller V1 and stronger imagery (Bergmann et al., 2016b). We therefore examined whether aphantasia is associated with thicker or larger V1.

No significant differences in cortical thickness or volume were observed in any early visual cortex region, with BFs yielding moderate evidence of group equivalence in both the calcarine cortex (Table S3) and V1 (Table S4). By contrast, whole-brain analysis revealed a single significant prefrontal cluster of reduced thickness in the left aPFC in aphantasia (Fig. 3A). Cluster statistics are reported in Table S5. Aphantasic individuals also showed greater cortical thickness in multiple medial temporal limbic regions, including left anterior parahippocampal gyrus and entorhinal cortex; right entorhinal cortex, retrosplenial cortex, posterior cingulate cortex. All statistical details are shown in Table S3. NODDI analysis identified higher NDI values in bilateral medial temporal regions and the left precuneus in aphantasia (Fig. S6), consistent with microstructural differences in these medial temporal regions.

To provide functional context for the observed thickness differences, we performed meta-analytic decoding of the t-map using Neurosynth (Fig. 3B). The left aPFC cluster showed strong associations with the terms “intentions” (r = 0.26), “actions” (r = 0.25), and “near (space)” (r = 0.25). Regions of increased thickness in aphantasia showed associations with anatomical terms including hippocampus, parahippocampus, and amygdala (all rs > 0.14), providing convergent functional annotation for the identified regions.

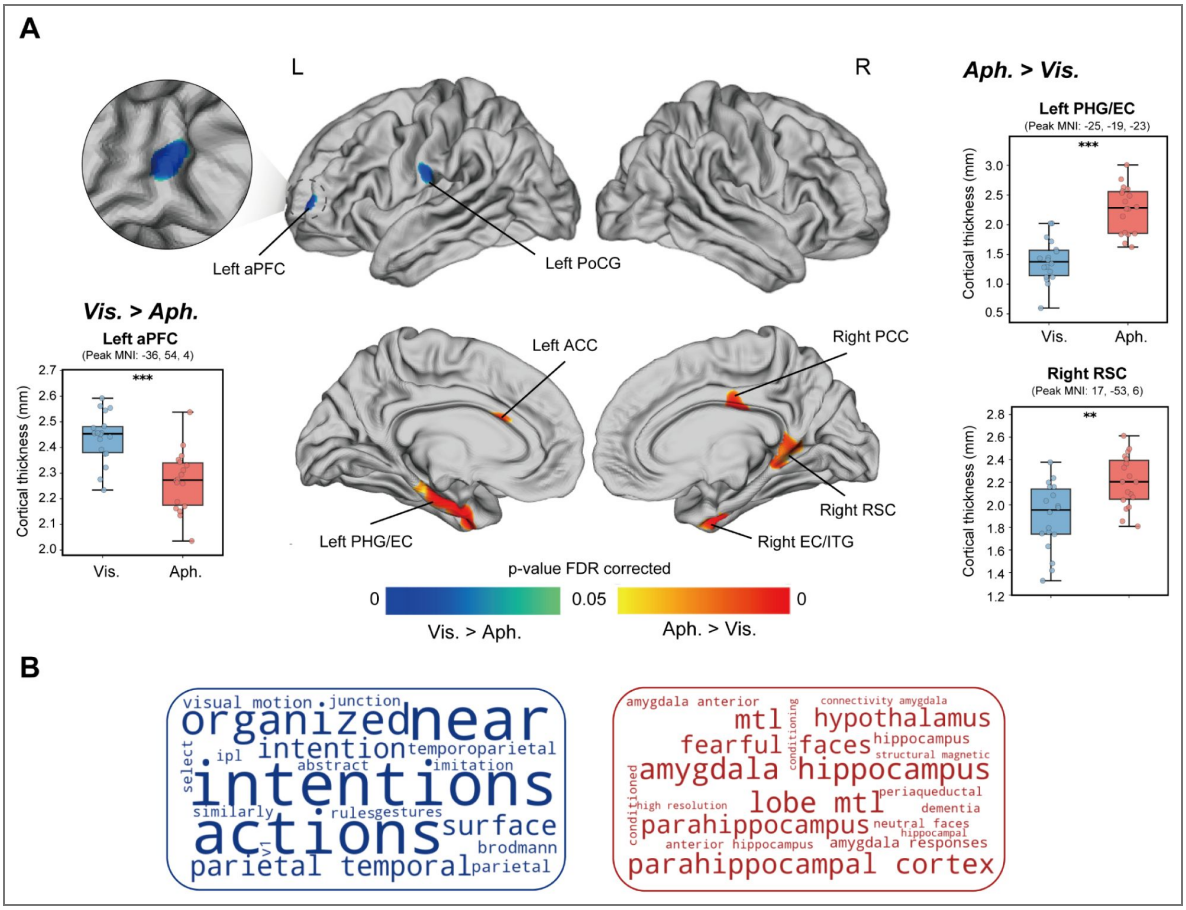

Figure 3. Regional differences in cortical thickness between aphantasic individuals and visualizers.

(A) Whole-brain t map of the group comparison. Blue indicates regions of reduced cortical thickness and red indicates regions of increased cortical thickness in aphantasia, with whole-cortex FDR correction. Boxplots show individual participant values (dots), median, and interquartile range. *p < 0.05, **p < 0.01, ***p < 0.001. Vis., visualizers; Aph., aphantasia. aPFC: anterior prefrontal cortex; PoCG: post central gyrus; PHG: parahippocampal gyrus; EC: entorhinal cortex; ITG: inferior temporal gyrus; RSC: retrosplenial cortex; PCC: posterior cingulate cortex. **(B)** Functional term associations derived from meta-analytic decoding of the t map using Neurosynth. Blue terms are associated with regions of reduced cortical thickness in aphantasia, and red terms with regions of increased cortical thickness. Term size reflects the strength of the Pearson correlation with the corresponding meta-analytic activation map.

Multivariate logistic regression

As an exploratory analysis, we used penalized multivariate logistic regression to identify the most parsimonious combinations of structural features associated with group separation. Separate models were fitted for FA, cortical thickness, and graph-theoretical measures, using only features showing group differences in the univariate analyses. The exploratory models showed strong in-sample discrimination, with all areas under the curve (AUCs) > 0.92. Across models, the strongest independent predictors of aphantasia were reduced FA in the right uncinate fasciculus and posterior interparietal corpus callosum, increased FA in the left dorsal cingulum, lower clustering coefficient in the left anterior insula, lower node strength in the left FEF, reduced left aPFC thickness, and greater anterior parahippocampal and retrosplenial cortical thickness. Full model statistics are reported in the Supplementary Materials.

Discussion

Congenital aphantasia has been proposed to reflect reduced functional coupling between higher-order prefrontal systems and high-level visual cortex, rather than a deficit in sensory representation alone (Liu & Bartolomeo, 2025). Here, we report structural findings that are, to our knowledge, the first direct anatomical evidence consistent with this account. Across tractometry, network analysis, and cortical morphometry, aphantasia was associated with a selective pattern of structural differences centered on higher-order fronto-temporal and cingulate systems, whereas we detected no reliable group differences in early visual cortex or in the major visual tracts examined.

Four converging observations characterize this structural phenotype. First, the UF and posterior interparietal corpus callosum showed reduced FA in aphantasia, implicating fronto-temporal and interhemispheric associative pathways. This pattern is consistent with prior functional findings of reduced coupling between OFC and anterior temporal regions in aphantasia (Liu et al., 2025a), two territories linked by the UF, potentially reflecting degraded binding between temporal mnemonic content and OFC affective and perceptual processing (Coad et al., 2020; Thomas et al., 2015). It may also be relevant to the broader behavioral profile reported in aphantasia, including altered autobiographical memory, face recognition, and emotional awareness (Zeman et al., 2020; Dawes et al., 2022; Monzel et al., 2024b), although direct structure-function relationships remain to be tested. Future studies should therefore assess these structural features alongside objective measures of episodic memory fidelity, face recognition, and affective processing.

Second, increased FA and neurite density in the dorsal cingulum are consistent with altered organization of a cognitive-control pathway. One possibility is that altered top-down regulation affects the conscious accessibility of internally generated representations, in a manner analogous to models of neurofunctional and psychiatric disorders (Mary et al., 2020; Kennis et al., 2015; Sasikumar & Strafella, 2021). Another is that these changes reflect compensatory reliance on semantically guided or non-visual control processes in aphantasia. Distinguishing between these possibilities will require task-based and longitudinal evidence.

Third, at the network level, aphantasia was associated with reduced local segregation in left anterior insula and altered connectivity metrics in frontal association regions, together with increased inter-network hubness in right dmPFC. These findings point to altered organization of attentional, salience, and default-mode systems. Given prior proposals implicating anterior insula and frontal control regions in the top-down regulation of internally generated representations, these network-level differences may affect conscious imagery construction at one or multiple stages (Liu, 2026): mediating inward attentional shifts (Nobre & Gresch, 2025), binding multiple features (Treisman, 2007), and gating conscious access (Huang et al., 2021). Along with the anterior cingulate cortex, insular alterations have also been proposed as a mechanism underlying some cases of acquired aphantasia, via reduced interoceptive and self-referential integration (Scholz et al., 2026).

Fourth, cortical thickness was selectively reduced in the left aPFC, a region which was found to be functionally disconnected in aphantasia (Liu & Bartolomeo, 2025), and whose grey-matter volume has previously been linked to imagery vividness in visualizers (Bergmann et al., 2016b). By contrast, cortical thickness was increased in medial temporal limbic regions, including the entorhinal (Moser et al., 2014) and retrosplenial cortex (Vann et al., 2009), critical for spatial navigation, episodic memory and imagined scene construction. Together with the tract and network findings, this pattern localizes the observed structural differences primarily to fronto-temporal and cingulate systems.

Across all four analyses, this structural dissociation is consistent with a recent multiple-stage model of conscious imagery and aphantasia (Liu, 2026), in which imagery experience depends on at least three broad operations: generation of internal visual representations, integration of distributed visual features into coherent object- or scene-like visual content (see also Scholz et al., 2025; Arcangeli & Bartolomeo, 2025), and amplification of that content for conscious access. Within this framework, the observed connectivity differences may affect integration and conscious access while leaving much of the sensory representational substrate relatively preserved.

In summary, this study provides the first comprehensive characterization of structural brain differences in congenital aphantasia, revealing a selective pattern centered on higher-order fronto-temporal and cingulate systems. By contrast, we found little evidence for major structural differences in early visual cortex or in its principal white-matter tracts, although the status of local U-shaped fibers (Guevara et al., 2020) remains to be determined. These findings argue that the structural basis of conscious imagery lies not in sensory representations themselves, but in the higher-order integrative and control systems that enable access to them.

Methods

Participants

Eighteen individuals with self-reported congenital aphantasia (mean ± SD age, 31.79 ± 12.11 years; 11 female) and 18 typical visualizers (32.29 ± 9.53 years; 15 female) were recruited. Ten aphantasic participants and five visualizers had also participated in a previous 7 Tesla fMRI study of mental imagery (Liu et al., 2025b). The sample size of 18 per group reflects the recruitment constraints inherent to congenital aphantasia, which affects an estimated 2–4% of the population. This is comparable to landmark structural MRI studies of analogous congenital conditions (Thomas et al., 2009). The convergent multimodal design and consistently large effect sizes (Cohen's d > 1.0) further support the sensitivity of the reported findings.

All participants completed the Vividness of Visual Imagery Questionnaire (VVIQ; Marks, 1973), which comprises 16 items rated from 1 ("no image at all") to 5 ("perfectly clear and as vivid as normal vision"), for a total score ranging from 16 to 80. All aphantasic participants had VVIQ scores below 22 (mean ± SD, 17.06 ± 2.10), and a lifelong absence of voluntary visual imagery was confirmed by structured interview conducted by J.L. No widely accepted objective diagnostic marker of congenital aphantasia is currently available (Bouyer et al., 2025). All visualizers had VVIQ scores above 50 (63.67 ± 9.54). All participants were right-handed, had normal or corrected-to-normal vision and hearing, and reported no history of neurological or psychiatric disorder. The two groups were matched for age, sex, and years of education. The study was approved by the institutional review board of INSERM (protocol C13-41), and all participants provided written informed consent in accordance with the Declaration of Helsinki.

Image acquisition

All MRI data were acquired at the Centre de NeuroImagerie de Recherche (CENIR), Paris Brain Institute, on a Siemens 3T MAGNETOM Prisma scanner equipped with a 64-channel head coil. Diffusion-weighted imaging (DWI) data were acquired across four sequences (398 volumes total), using two phase-encoding directions (anterior-to-posterior, AP; posterior-to-anterior, PA), each with 98-99 uniformly distributed diffusion directions at two b values (b = 1,500 and 3,000 s/mm²).

In addition, 28 non-diffusion-weighted (b = 0) volumes were acquired. High-resolution T1-weighted anatomical images were acquired in the same session (TR = 2,400 ms, TE = 2.22 ms, flip angle = 9°).

DWI and T1-weighted data processing

Grey matter/white matter segmentation

Anatomical T1-weighted images were preprocessed using the DeepPrep 25.1.0 pipeline (Ren et al., 2025), which combines deep-learning-based and established neuroimaging tools for robust tissue segmentation. Processing included motion correction using FreeSurfer (v7.2.0; *RRID:SCR_001847*), bias-field correction using SimpleITK (v2.3.0), skull stripping and tissue segmentation using FastSurferCNN from FastSurfer (v1.1.0), and cortical surface reconstruction using FastCSR (v1.0.0). The preprocessed T1-weighted image served as the anatomical reference for subsequent diffusion-weighted analyses.

Diffusion-weighted image preprocessing

Diffusion-weighted images were preprocessed using QSIPrep v1.0.2 (Cieslak et al., 2021) with default parameters. Sequences with the same phase-encoding polarity were merged before preprocessing. The pipeline included MP-PCA denoising, Gibbs-ringing removal, intensity normalization across b = 0 images, N4 bias-field correction, and correction for head motion, eddy currents, and susceptibility-induced distortion using FSL's eddy and TOPUP, with outlier replacement enabled. Final interpolation used Jacobian modulation, and the data were resampled to each participant's native AC-PC space at 1.25 mm isotropic resolution.

Fiber reconstruction

Preprocessed DWI data were reconstructed using QSIRecon v1.0.1 (Cieslak et al., 2021) with the *mrtrix_multishell_msmt_ACT-hsvs* workflow. Brain masks from *antsBrainExtraction* were used throughout reconstruction. Multi-tissue response functions were estimated using the Dhollander algorithm, and white-matter fiber orientation distributions (FODs) were computed using multi-tissue constrained spherical deconvolution and intensity-normalized with *mtnormalize*. These FODs were used for tractography, whereas anatomical constraints were derived from T1-weighted hybrid surface-volume segmentation (hsvs) to generate five-tissue-type images. Whole-brain tractography was then performed using anatomically constrained tractography (ACT), with streamlines constrained to initiate and terminate at the grey-white matter interface. SIFT2 was applied to estimate per-streamline weights, which were retained for subsequent bundle segmentation and connectivity analyses.

Bundle segmentation

White-matter fascicles of interest were identified using pyAFQ (Kruper et al., 2021) within QSIRecon, following the *mrtrix_multishell_msmt_pyafq_tractometry* workflow without re-running ACT. In addition to the standard major fiber bundles included in pyAFQ, several custom tracts were defined for hypothesis-driven analyses using region-of-interest (ROI) definitions from prior studies. These included superior longitudinal fasciculus subdivisions (Thiebaut de Schotten et al., 2011) (SLF I, II, IIIi) and ventral cingulum pathways containing posterior cingulate and medial temporal projections (Warrington et al., 2020). All ROIs were transformed into each participant's native AC-PC space. Association fibers were constrained to remain within the hemisphere, and bundle refinement was performed using iterative outlier removal and streamline clustering.

Tractometry

For each segmented bundle, tract profiles were extracted by resampling streamlines to 100 equidistant nodes using the pyAFQ workflow. Node-wise diffusion and microstructural metrics were then computed as weighted averages across streamlines, including fractional anisotropy (FA), mean diffusivity (MD), radial diffusivity (RD), axial diffusivity (AD), and neurite orientation dispersion and density imaging (NODDI) parameters. FA is sensitive to overall fiber organization but does not distinguish between true microstructural differences and geometric effects such as

crossing, fanning, or bending fibers (Sotiropoulos & Zalesky, 2019). To aid interpretation, we therefore also quantified NODDI-derived neurite density index (NDI) and orientation dispersion index (ODI), which provide more specific estimates of tissue microstructure (Zhang et al., 2012). NODDI was fitted using the AMICO implementation in QSIRecon, with parallel diffusivity fixed at 1.7×10^{-3} mm²/s and isotropic diffusivity at 3.0×10^{-3} mm²/s. NDI and ODI values were computed at each node along the tract profiles. Prior to group-level statistical analysis, tract profiles were smoothed along the tract using a 3-node full-width at half maximum (FWHM) kernel.

fROI fiber tracking

Four ROIs from a core mental imagery network were extracted from a previous 7 Tesla fMRI study of aphantasia (Liu et al., 2025b) : the fusiform imagery node (FIN), left anterior prefrontal cortex (aPFC), left orbitofrontal cortex (OFC), and right anterior intraparietal sulcus (aIPS). In aphantasic individuals, these ROIs showed altered functional connectivity or activity, motivating the analysis of their white-matter connections. Group-level ROIs were transformed into each participant's native AC-PC space. To avoid overestimation of ROI size, volumetric fROIs were projected onto the cortical surface using FreeSurfer (*RRID:SCR_001847*) and mapped to the grey-white matter interface (Meisler et al., 2024). The streamline search space was defined as the intersection between the projected fROIs and the grey-white matter interface mask. Streamlines intersecting this region were identified using MRtrix3 (mrcalc) with the default radial endpoint search radius of 2 mm. For each ROI, streamlines were extracted and quantified in native space using two indices: the proportion of streamlines assigned to each anatomically defined bundle, and the number of streamlines normalized by ROI volume. Bundles of interest were defined according to the anatomical location of each ROI. For the FIN, these included the long segment of the arcuate fasciculus (AF), posterior arcuate fasciculus (pAF), inferior fronto-occipital fasciculus (IFOF), inferior longitudinal fasciculus (ILF), and vertical occipital fasciculus (VOF). For the left aPFC and left OFC, the bundles of interest were the IFOF and uncinate fasciculus (UF). For the right aIPS, the bundles of interest were the pAF and SLF I, II, and III. Group differences were assessed using both normalized streamline counts and bundle-wise streamline proportions.

Graph-theoretic network analysis

Cortical parcellation was performed using the Schaefer 400-parcel, 17-network atlas (Schaefer et al., 2018), registered from template space to individual DWI space via T1-weighted normalization. Structural connectivity between parcel pairs was estimated by intersecting the endpoints of SIFT2-weighted streamlines with parcel ROIs. A streamline was assigned to a parcel pair if both endpoints fell within a 2 mm radius sphere centered on the corresponding parcel centroids. Connection strength was defined as the sum of SIFT2 weights across all streamlines linking a parcel pair, normalized by parcel volume to account for region-size differences. Symmetric adjacency matrices were generated for each participant and thresholded using consensus thresholding (de Reus & van den Heuvel, 2013), such that connections absent in at least 50% of participants in either group were set to zero. Graph-theoretic metrics were computed on weighted, undirected networks using the Brain Connectivity Toolbox (Rubinov & Sporns, 2010) in MATLAB R2024b (*RRID:SCR_001622*). The metrics examined were node strength, clustering coefficient, global efficiency, betweenness centrality, and participation coefficient. To assess robustness across parcellation schemes, analyses were repeated using the Schaefer 100-parcel and Gordon 333-parcel functional atlases.

Surface extraction and surface-based morphometry

Surface-based morphometry was conducted using the Computational Anatomy Toolbox (CAT12) implemented in SPM12 (Gaser et al., 2024). Cortical thickness was estimated using CAT12's default projection-based method, which computes the distance between the inner cortical surface (grey-white matter boundary) and the outer cortical surface (grey matter-cerebrospinal fluid boundary). Individual cortical thickness maps were smoothed with a 12 mm FWHM Gaussian kernel and resampled to the 32k surface before statistical analysis. Whole-brain statistical analysis

was performed in CAT12. The resulting t maps were then used as input for Neurosynth (*RRID:SCR_006798*) decoding in BrainStat to compute Pearson correlations with meta-analytic activation maps. The 20 strongest term correlations were retained for visualization.

To examine the visual cortex specifically, we used two atlas-based approaches. Grey matter volume was extracted from occipital regions using the Neuromorphometrics atlas (*RRID:SCR_005656*) as implemented in CAT12, and cortical thickness was extracted from early visual regions using the HCP-MMP Glasser atlas. Grey matter volume measures were normalized by total intracranial volume to account for individual differences in head size.

Quantification of NODDI in grey matter and white-matter tracts

To complement cortical thickness analysis with microstructurally interpretable measures, NODDI metrics were also quantified in cortical grey matter. NODDI was fit using the AMICO implementation described above, and volumetric NDI and ODI maps were sampled onto the cortical surface uniformly between the pial and white matter boundaries using Nilearn's *vol_to_surf* function, then resampled to the fsLR-32k surface. The NODDI model has been validated against histological measures in both grey and white matter, and ODI has been shown to be sensitive to microstructural changes including demyelination in post-mortem tissue.

Logistic regression

To identify parsimonious combinations of structural features associated with group membership while accounting for shared variance across measures, we used a two-step modelling approach. First, LASSO-penalized logistic regression (*glmnet* package in R) was applied separately within each metric domain: tractometry FA, cortical thickness, and graph-theoretic measures. Predictors comprised mean FA across significant tract nodes, cortical thickness values, and graph metrics identified in prior analyses. Separate domain-specific models were used to limit the predictor-to-sample ratio given the modest sample size (N = 36). Model selection was performed using 5-fold cross-validation with approximately balanced class distributions, and the regularization parameter was chosen using the 1-standard-error rule ($\lambda_1$se). In a second step, variables retained by LASSO were entered into Firth's penalized logistic regression (Firth, 1993) to obtain bias-reduced parameter estimates and odds ratios, thereby reducing small-sample bias and separation problems. Variables that caused non-convergence were excluded using a p-value-based stepwise procedure.

Statistical analysis

Bayes factors

To quantify evidence for and against group differences, we computed Bayes factors (BFs) in JASP (*https://jasp-stats.org/*; *RRID:SCR_015823*) using Bayesian t tests and Mann-Whitney U tests with default priors on effect size. BF10 > 3 was taken as moderate evidence for a group difference, whereas BF01 > 3 (equivalently, BF10 < 1/3) was taken as moderate evidence for the absence of a group difference (Keysers et al., 2020).

Tractometry

Group differences in tract profiles were assessed using one-dimensional threshold-free cluster enhancement (TFCE; E = 0.5, H = 2) along tract nodes, implemented in PALM with 10,000 permutations. TFCE identifies spatially extended effects without requiring an arbitrary cluster-forming threshold and assigns a family-wise-error-corrected p value to each node. To reduce spurious findings, only clusters comprising at least 3 consecutive significant nodes were reported. Statistical significance was defined as $p < 0.05$, FWE-corrected.

Graph-theoretic network analysis

Group differences in node-level graph-theoretic metrics were assessed using the non-parametric Brunner-Munzel test, with false-discovery-rate correction applied across all nodes within each metric. The same test was also used to assess group differences in SIFT2-weighted streamline

counts between ROI pairs.

fROI fiber tracking

Group differences in filtered tracts within each fROI were assessed using the Mann-Whitney test, because the data included a substantial number of zero values and did not satisfy the assumptions of parametric testing.

Surface-based morphometry

Statistical analyses of cortical thickness were performed in BrainStat (Larivière et al., 2023) using a linear model with a one-sided test and false discovery rate (FDR) correction. To identify spatially coherent clusters of significant vertices, hierarchical density-based spatial clustering of applications with noise (HDBSCAN) was applied to the x-, y-, and z-coordinates of significant vertices, grouping those that were spatially adjacent. Only clusters containing at least 30 vertices were retained for interpretation, and Desikan killiany atlas was used to identify the anatomical region of surviving clusters.

Grey matter NODDI

Cortical grey matter NODDI metrics were compared between groups using random field theory as implemented in BrainStat (Larivière et al., 2023). Cluster-level inference used a cluster-forming threshold of $p < 0.05$ and a cluster-significance threshold of $p < 0.05$, FWE-corrected.

Data availability

Requests for materials and correspondence should be addressed to the lead contact Jianghao Liu.

Supplementary materials

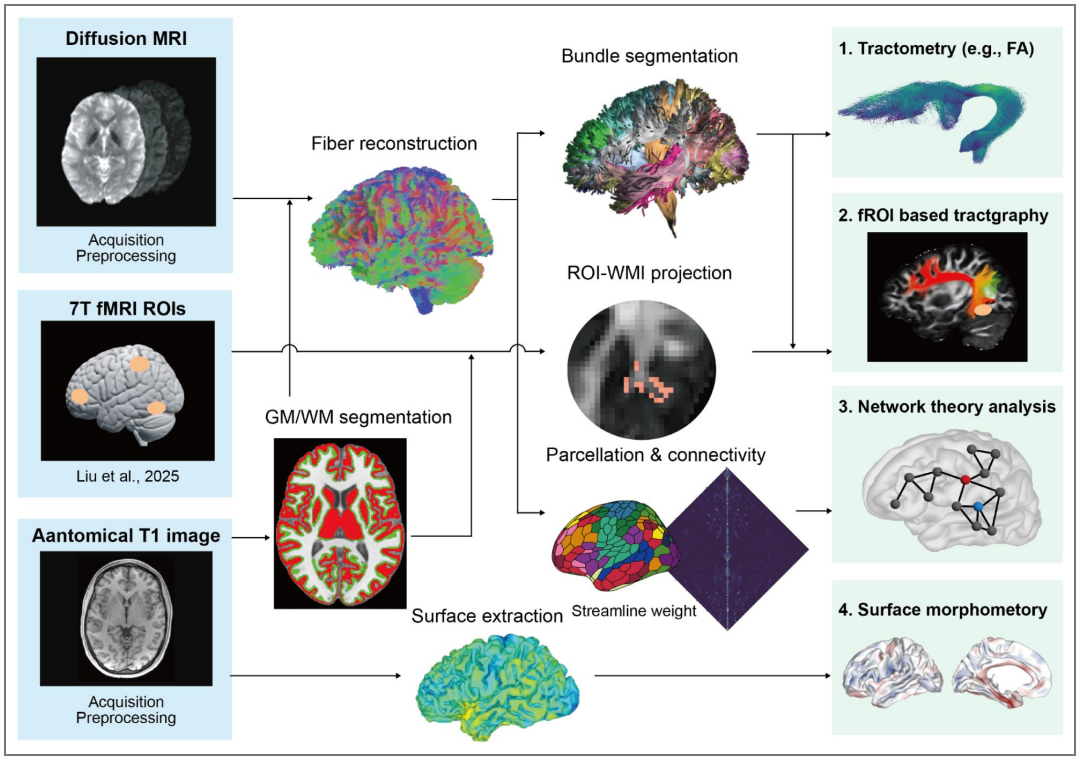

Supplementary Figure S1. Overview of the analysis pipeline. Three data streams were processed in parallel. Diffusion MRI data underwent preprocessing and fiber reconstruction to generate whole-brain tractography. Anatomical T1-weighted images were processed for grey matter/white matter (GM/WM) segmentation and cortical surface extraction. Functional ROIs from a previous 7T fMRI study of mental imagery (Liu et al., 2025b) were registered to each participant's native space. These inputs were then used for four complementary analyses:

(1) tractometry, in which white-matter bundles were segmented and microstructural properties, including fractional anisotropy (FA), were quantified along tract profiles; **(2) fROI-based tractography**, in which functional ROIs were projected to the GM/WM interface to identify streamlines connecting regions of the core imagery network; **(3) graph-theoretic network analysis**, in which cortical parcellation and SIFT2-weighted streamline counts were used to construct structural connectivity matrices and derive node-level network metrics; and **(4) surface morphometry**, in which cortical thickness was estimated from the extracted cortical surfaces and compared between groups across the whole brain.

Axial and radial diffusivity and NODDI control analyses for tractometry findings

To clarify the potential biological basis of the FA differences, we examined axial diffusivity (AD) and radial diffusivity (RD), often interpreted as being more sensitive to axonal and myelin-related properties, respectively (Song et al., 2002), together with neurite orientation dispersion and density imaging (NODDI) metrics, including neurite density index (NDI) and orientation dispersion index (ODI) (Zhang et al., 2012), at all segments showing significant FA effects. Full statistics are reported in Table S1.

Uncinate fasciculus and posterior interparietal corpus callosum

FA reductions in the bilateral uncinate fasciculus and posterior interparietal corpus callosum were accompanied by marginal RD increases at largely overlapping segments (all $p < 0.1$, FWE-corrected), a pattern consistent with altered myelin-related microstructure. No significant group differences in NDI or ODI were observed at the same segments, suggesting that these FA reductions are unlikely to be explained by fiber-geometry effects such as crossing fibers.

Bilateral dorsal cingulum

The FA increase in the bilateral dorsal cingulum was accompanied, in the left hemisphere, by a significant RD decrease and AD increase, consistent with altered microstructural organization rather than myelin degradation. A significant increase in NDI was observed at the same segments showing elevated FA, with no change in ODI, suggesting that the FA increase is more likely to reflect greater neurite density than reduced fiber dispersion.

Marginal findings

Marginal FA reductions were observed in the right SLF-II (Fig. S3A; $p = 0.082$) and right ventral cingulum ($p = 0.079$). Both tracts also showed increased ODI at the same segments (Fig. S3B), suggesting that these marginal effects may be influenced by local fiber geometry rather than robust microstructural differences. We therefore did not interpret these findings further.

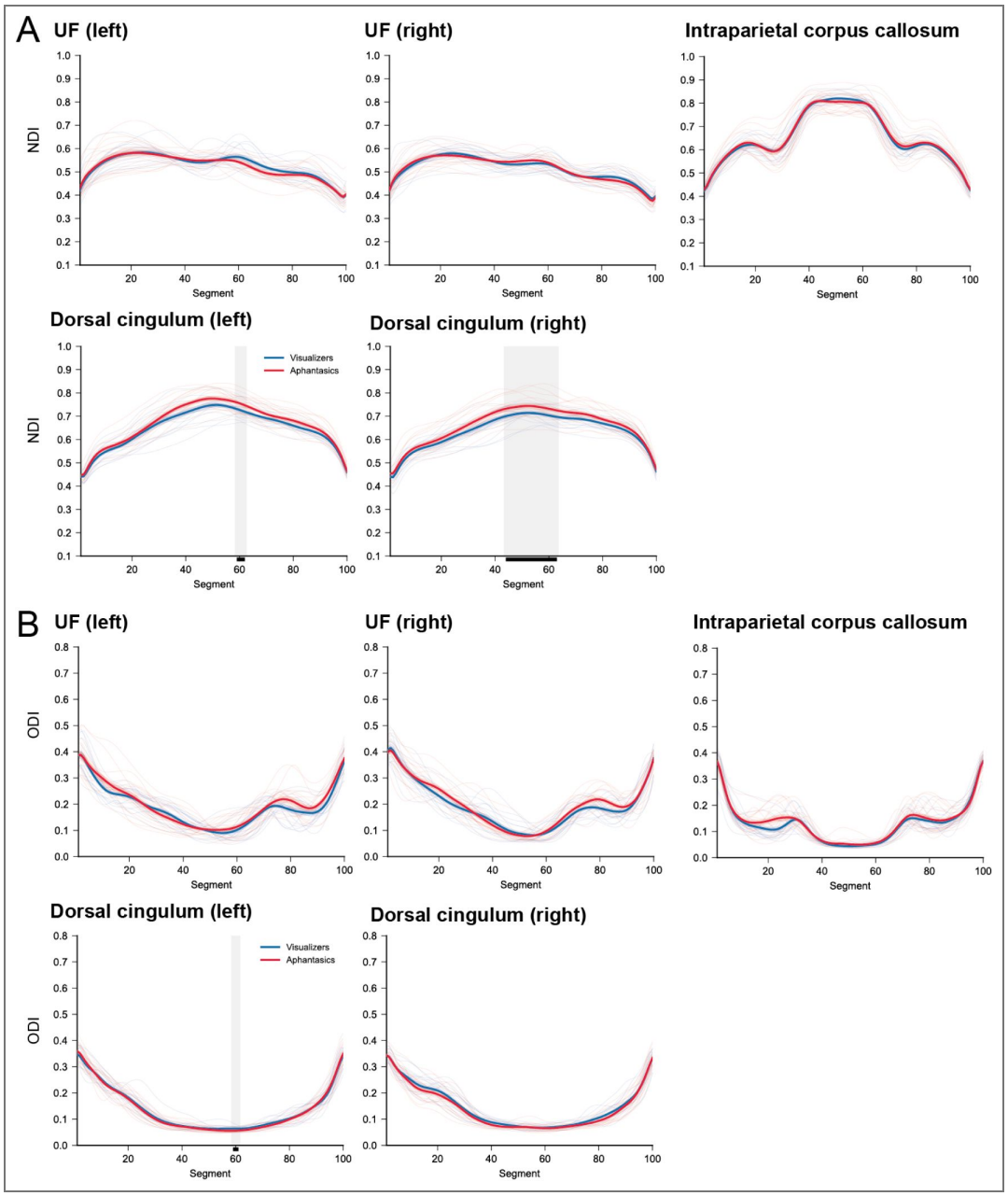

Supplementary Figure S2. NODDI microstructural profiles in white-matter tracts showing significant FA differences. (A) Neurite density index (NDI) tract profiles. **(B)** Orientation dispersion index (ODI) tract profiles. Profiles are shown for the bilateral uncinate fasciculus, posterior interparietal corpus callosum, and bilateral dorsal cingulum, the tracts identified in the main tractometry analysis. Red lines indicate aphantasic individuals and blue lines indicate visualizers. Thin lines show individual participant profiles; thick lines show group means ± SEM. Shaded grey regions and black bars indicate significant between-group differences ($p < 0.05$, FWE-corrected).

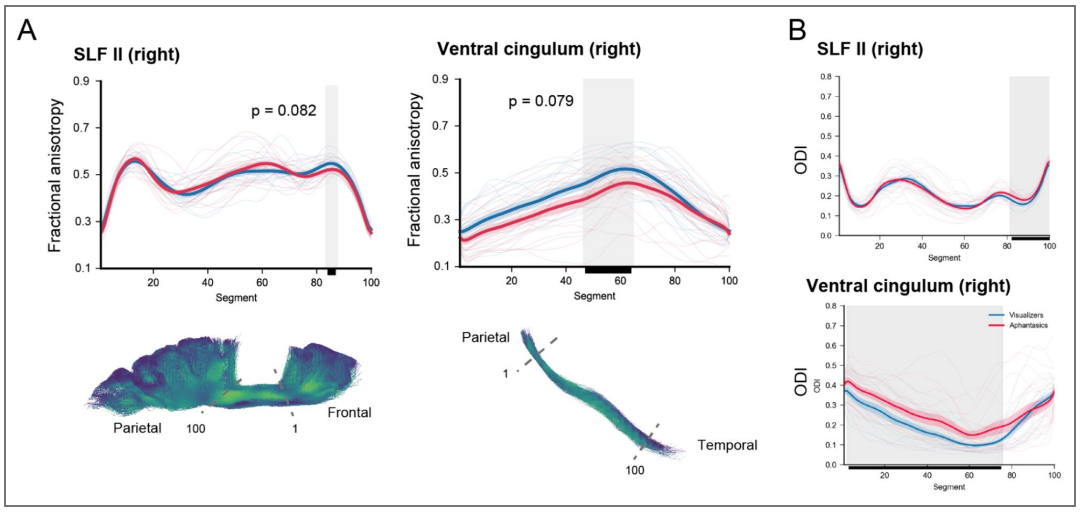

Supplementary Figure S3. Marginal FA reductions in the right SLF-II and right ventral cingulum are accompanied by increased orientation dispersion. (A) Fractional anisotropy (FA) tract profiles for the right SLF-II (p = 0.082, FWE-corrected) and right ventral cingulum (p = 0.079, FWE-corrected), with representative tract reconstructions shown below. Shaded grey regions and black bars indicate segments showing marginal between-group differences. Red lines indicate aphantasic individuals and blue lines indicate visualizers; thin lines show individual participant profiles and thick lines show group means ± SEM. **(B)** Orientation dispersion index (ODI) profiles for the same tracts. In both tracts, marginal FA reductions overlapped with increased ODI in aphantasic individuals, suggesting that these effects may be influenced by local fiber geometry rather than robust microstructural differences. These findings were therefore not interpreted further.

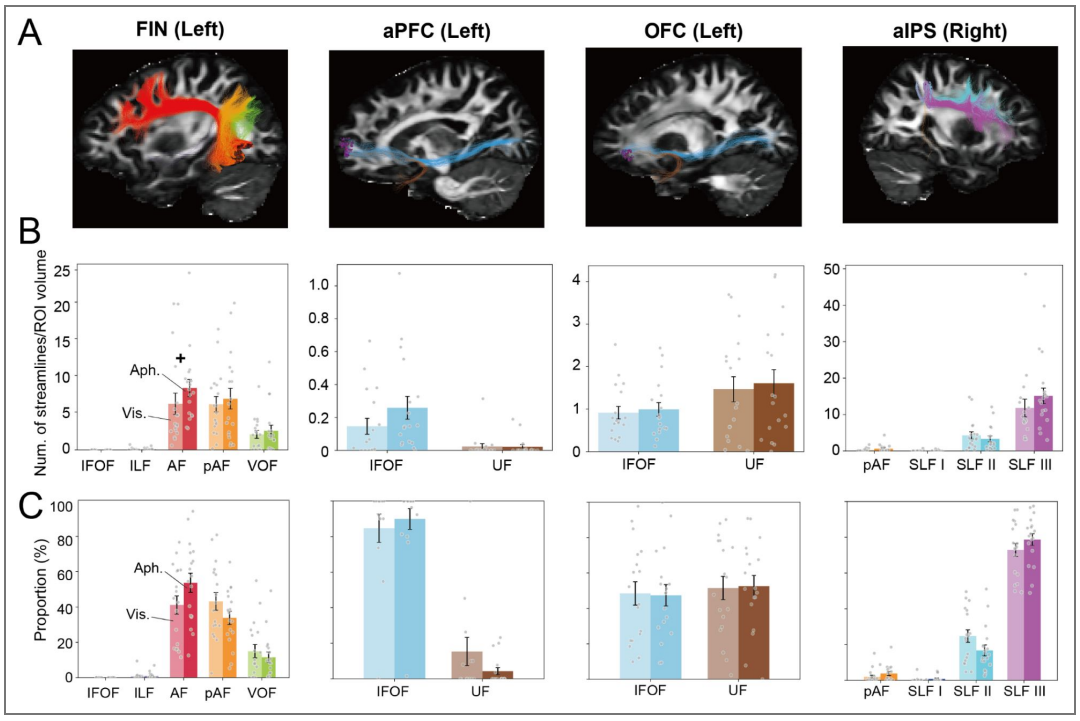

Supplementary Figure S4. White-matter connections of the core imagery network. (A) White-matter streamlines associated with each functional ROI of the core imagery network, shown on sagittal MRI sections: left fusiform imagery node (FIN), left orbitofrontal cortex (OFC), left anterior prefrontal cortex (aPFC), and right anterior intraparietal sulcus (aIPS). **(B)** Streamline counts normalized by ROI volume for each functional ROI. The FIN was connected primarily by the long segment of the arcuate fasciculus (AF), posterior arcuate fasciculus (pAF), and vertical occipital fasciculus (VOF). The left OFC was connected by both the inferior fronto-occipital fasciculus (IFOF) and uncinate fasciculus (UF), whereas the left aPFC was connected mainly by the IFOF. No direct structural connection was identified between the FIN and left aPFC in this analysis. The right aIPS was connected

predominantly by the third branch of the superior longitudinal fasciculus (SLF-III). A nominal increase in normalized streamline count was observed in aphantasic individuals for the left AF associated with the FIN (uncorrected p = 0.039, U = 229, Cliff's d = -0.41), but this effect did not survive correction for multiple comparisons. Bayes factor analysis provided moderate evidence for no group difference in VOF streamline count associated with the FIN (BF = 0.32). **(C)** Proportion of streamlines assigned to each tract of interest for each ROI. Light bars indicate visualizers and dark bars indicate aphantasic individuals. Error bars show SEM and dots indicate individual participants. IFOF, inferior fronto-occipital fasciculus; ILF, inferior longitudinal fasciculus; AF, arcuate fasciculus long segment; pAF, posterior arcuate fasciculus; VOF, vertical occipital fasciculus; UF, uncinate fasciculus; SLF-I/II/III, superior longitudinal fasciculus branches I, II, and III.

Control analysis on atlas selection in network analysis

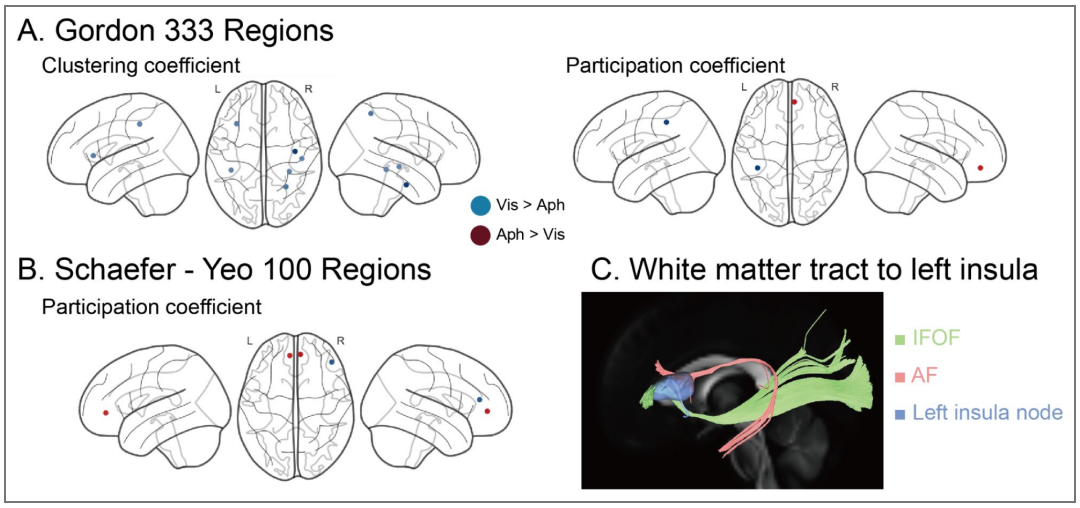

Supplementary Figure S5. Control analyses confirm the robustness of network findings across parcellation schemes. (A) Gordon 333-region atlas. Convergent group differences were observed across graph-theoretic metrics, with aphantasic individuals showing reduced clustering coefficient in the left anterior insula (Vis. > Aph., blue) and increased participation coefficient in the right dorsomedial prefrontal cortex (dmPFC; Aph. > Vis., dark red). **(B)** Schaefer-Yeo 100-region atlas. Aphantasic individuals showed increased participation coefficient in bilateral dmPFC (Aph. > Vis.) and reduced participation coefficient in right lateral prefrontal cortex (Vis. > Aph.). **(C)** White-matter tracts connected to the left anterior insula node in the Schaefer-Yeo 400-region atlas. The inferior fronto-occipital fasciculus (IFOF) and arcuate fasciculus (AF) converge on the left anterior insula, the node showing reduced clustering coefficient in the main analysis. The left anterior prefrontal cortex (aPFC) and fusiform imagery node (FIN) are linked by distinct white-matter pathways, primarily IFOF and AF, respectively. Dark red indicates Aph. > Vis. and blue indicates Vis. > Aph. All group differences shown in panels A and B were significant at $p < 0.05$, FDR-corrected. The left frontal eye field (FEF) was not identified consistently across atlases, consistent with uncertainty in its parcellation boundaries.

Control analysis on NODDI gray matter

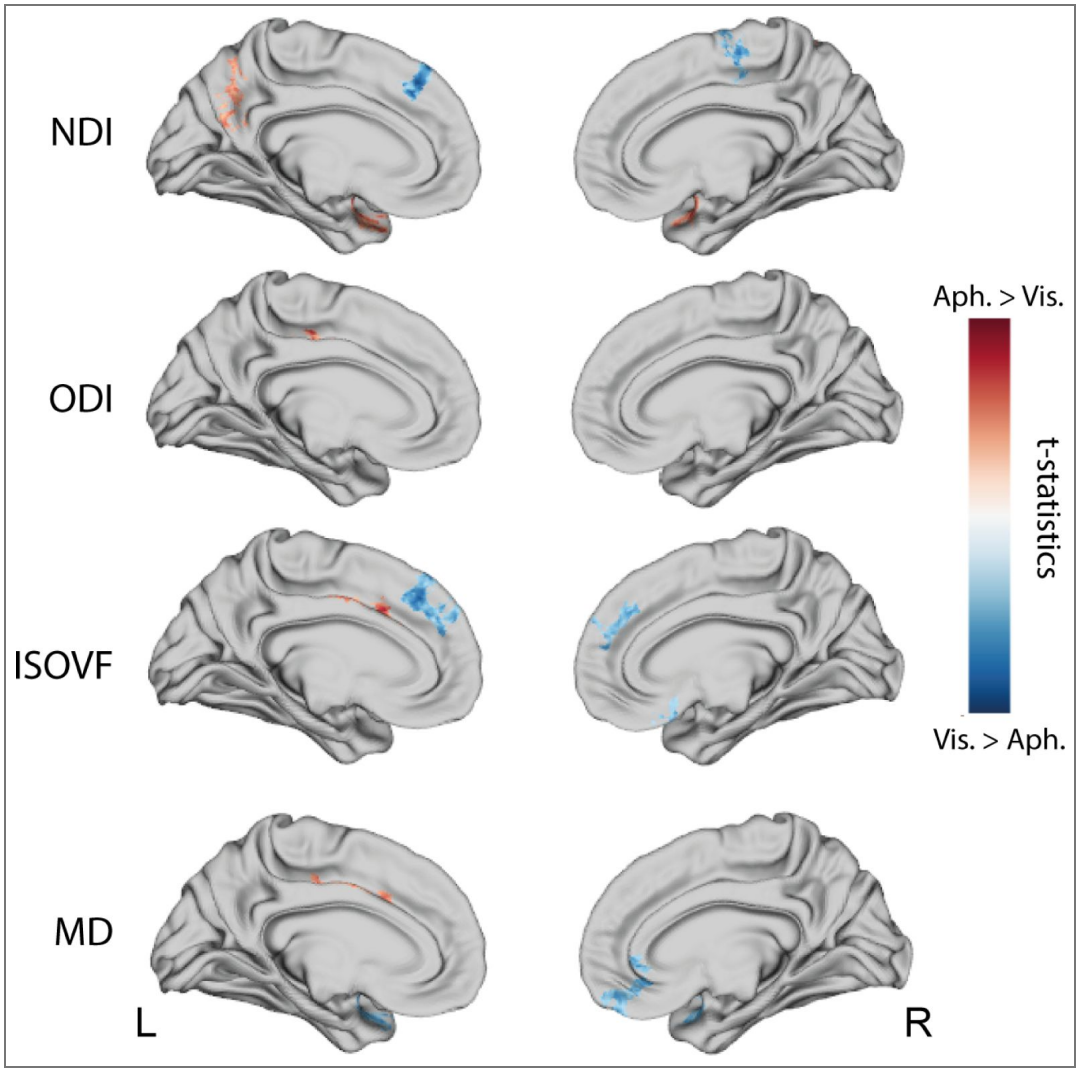

Supplementary Figure S6. Cortical NODDI microstructural differences between aphantasic individuals and visualizers. Cortical NODDI metrics were compared between groups using random field theory as implemented in BrainStat, with cluster-level FWE correction ($p < 0.05$). Aphantasic individuals showed increased neurite density index (NDI) in bilateral medial temporal regions, including the parahippocampal gyrus and entorhinal cortex, as well as in the left precuneus, and reduced NDI in the left dorsomedial prefrontal cortex. Orientation dispersion index (ODI), isotropic volume fraction (ISOVF), and mean diffusivity (MD) also showed significant group differences. Regions of reduced MD overlapped spatially with areas of increased NDI in medial temporal cortex, a pattern consistent with denser neurite packing and lower overall diffusivity in these regions.

		DTI			NODDI	
Tract		**Fractional anisotropy (FA)**	**Axial diffusivity (AD)**	**Radial diffusivity (RD)**	**Neurite density index (NDI)**	**Orientation dispersion index (ODI)**
		Vis > Aph		*Aph > Vis*		
right UF		77-84 (0.018; 3.43; 1.14)		78-83 (0.061; 2.50; 0.83)		
left UF		75-77 (0.048; 2.89; 0.96)		74-78 (0.085; 2.54; 0.85)		
interparietal corpus callosum		47-50 (0.039; 3.01; 1.00)		47-52 (0.071; 2.71; 0.90)		
		Aph > Vis	*Aph > Vis*	*Vis > Aph*	*Aph > Vis*	*Vis > Aph*
right cingulum	dorsal	46-69(0.019; 2.85; 0.95)		40-76 (0.016; 2.96; 0.99)	44-63 (0.046; 2.17; 0.72)	
left cingulum	dorsal	39-68 (0.003; 3.95; 1.32)	52-61 (0.068; 2.51; 0.84)	30-69 (0.004; 3.78; 1.26)	59-62 (0.047; 2.50; 0.83)	59-61(0.041; 3.00; 1.00)

Supplementary Table S1. Tract-level diffusion and NODDI differences between aphantasic individuals and visualizers. Significant group differences in tract-profile diffusion tensor imaging (DTI) and neurite orientation dispersion and density imaging (NODDI) metrics are shown for tracts identified in the tractometry analysis. Values indicate the start and end nodes of each significant cluster, followed by the FWE-corrected p value, test statistic, and Cohen's d in parentheses. Direction of effect is indicated separately for each metric column (Vis. > Aph. or Aph. > Vis.). Only clusters meeting the reporting threshold of at least 3 consecutive significant nodes are listed. For the main analyses, significance was defined as $p < 0.05$, FWE-corrected; marginal effects ($p < 0.1$, FWE-corrected) are reported in the text but are not included in this table.

Metric	Node (Network)	MNI coordinates (x, y, z)	B-M statistic	p (FDR corrected)	Cliff's delta
Vis. > Aph.					
Strength	Left FEF (DAN B)	25, -1, 55	-4.33	0.050	0.65
Clustering coefficient	Left anterior insula (Salience/VAN A)	-33, 18, 6	-7.18	<0.001	0.77
Clustering coefficient	Left dlPFC (Default B)	-42, 7, 48	-4.93	0.004	0.66
Participation coefficient	Right somatomotor (SomMot B)	9, -40, 68	-4.05	0.038	0.59
Aph. > Vis.					
Participation coefficient	Right dmPFC (Default A)	7, 42, 4	4.64	0.024	-0.66
Participation coefficient	Right dmPFC (Default A)	7, 54, 13	4.19	0.038	-0.63

Supplementary Table S2. Nodal graph-theoretic network differences between aphantasic individuals and visualizers. Significant group differences in nodal graph-theoretic metrics are reported for node strength, clustering coefficient, and participation coefficient. Group comparisons were performed using the Brunner-Munzel test with false discovery rate (FDR) correction within each metric. MNI coordinates (x, y, z) correspond to parcel centroids. Network affiliations are defined according to the Schaefer 400-parcel, 17-network atlas. **Vis. > Aph.** indicates lower metric values in aphantasic individuals, whereas **Aph. > Vis.** indicates higher metric values in aphantasic individuals. **B-M statistic** denotes the Brunner-Munzel statistic, and **Cliff's delta** the effect size. Significance threshold: $p < 0.05$, FDR-corrected.

Region	Aphantasics (× 10^-4 mm³/TIV)	Visualizers (× 10^-4 mm³/TIV)	BF+0
Right calcarine cortex	20 ± 2.26	20 ± 2.70	**0.21***
Left calcarine cortex	20 ± 2.71	20 ± 2.35	**0.22***
Right inferior occipital gyrus	40 ± 2.50	40 ± 3.15	0.35
Left inferior occipital gyrus	30 ± 2.97	30 ± 3.74	0.33
Right lingual gyrus	50 ± 4.74	50 ± 3.72	0.75
Left lingual gyrus	50 ± 2.87	50 ± 3.65	0.59
Right middle occipital gyrus	30 ± 3.50	30 ± 2.84	**0.23***
Left middle occipital gyrus	40 ± 4.50	40 ± 2.94	**0.33***
Right occipital pole	20 ± 2.94	20 ± 2.67	0.42
Left occipital pole	20 ± 2.18	20 ± 2.21	**0.28***
Right occipital fusiform gyrus	20 ± 2.10	20 ± 2.13	0.92
Left occipital fusiform gyrus	20 ± 1.89	20 ± 2.10	0.37

Note: For all Bayesian tests, the alternative hypothesis specified smaller regional volume in visualizers than in aphantasics. ***BF10 < 0.33**, indicating moderate evidence for the null hypothesis.

Supplementary Table S3. Gray matter volume in occipital cortical regions. Regions were defined using the Neuromorphometrics atlas in CAT12. Gray matter volumes were normalized by total intracranial volume (TIV). No significant group differences were observed in any occipital cortical region. Bayes factors provided moderate evidence for an equal volume between the two groups in the left and right calcarine cortices. Values are reported as mean ± SD.

Region	Aphantasics (mm)	Visualizers (mm)	BF+0
lV1	1.83 ± 0.11	1.86 ± 0.13	**0.21***
rV1	1.83 ± 0.10	1.82 ± 0.15	0.37
lV2	1.94 ± 0.09	1.96 ± 0.11	**0.21***
rV2	1.94 ± 0.10	1.93 ± 0.13	0.37
lV3	2.10 ± 0.10	2.11 ± 0.13	**0.30***
rV3	2.03 ± 0.12	2.07 ± 0.11	0.17

Note: For all Bayesian tests, the directional alternative specified greater cortical thickness in aphantasia than in visualizers. *BF_{10} < 0.33.

Supplementary Table S4. Cortical thickness in early visual areas in aphantasic individuals and visualizers. Mean cortical thickness values (mm ± SD) for atlas-defined early visual regions are shown for the aphantasia and visualizer groups. Regions of interest were defined using the HCP-MMP atlas. No significant group differences were observed in any region. Bayes factors indicated moderate evidence for the absence of a group difference in 4 of the 6 regions (BF_{+0} < 0.33). l, left hemisphere; r, right hemisphere.

Region	Cluster size	Peak t-value	Peak p-value (FDR)	MNI coordinates (x, y, z)	Cohen's D
Vis. > Aph.					
Left aPFC	52	4.68	0.000	-36, 54, 4	1.56
Left PoCG	49	3.73	0.005	-64, -14, 22	1.24
Aph. > Vis.					
Left PHG/EC	264	6.83	0.000	-25, -19, -23	2.28
Left ACC	44	3.61	0.005	-4, 18, 23	1.20
Right RSC	294	3.52	0.007	17, -53, 6	1.17
Right EC/IFG	145	4.49	0.000	32, -6, -38	1.50
Right PCC	110	4.41	0.001	5, -18, 29	1.47

Supplementary Table S5. Cortical thickness differences between aphantasic individuals and visualizers. Significant group differences in cortical thickness are reported for clusters comprising more than 30 vertices. Group comparisons were performed using a linear model with FDR correction. aPFC: anterior prefrontal cortex; PoCG: Post central gyrus; PHG: parahippocampal gyrus; EC: Entorhinal cortex; ACC: Anterior cingulate cortex; RSC: retrosplenial cortex; PCC: Posterior cingulate cortex.

Multiple regression model

We used a two-step modelling approach. First, LASSO-penalized logistic regression was applied separately within each metric domain to identify the most informative predictors. Second, the variables retained by LASSO were entered into Firth's penalized logistic regression to obtain bias-reduced parameter estimates and odds ratios.

For the tractometry model, LASSO logistic regression retained the left dorsal cingulum, right uncinate fasciculus, and posterior interparietal corpus callosum at $\lambda_1$se. In the Firth model, higher FA in the right uncinate fasciculus was marginally associated with lower odds of aphantasia (beta = −1.00; OR = 0.36, 95% CI = 0.07-1.00; p = 0.051), as was higher FA in the posterior interparietal corpus callosum (beta = −1.70; OR = 0.18, 95% CI = 0.02-0.61; p = 0.003). Higher FA in the left dorsal cingulum was significantly associated with increased odds of aphantasia (beta = 1.79; OR = 6.03, 95% CI = 1.79-51.40; p < 0.001). These multivariate results were broadly consistent with the tract-level univariate findings. Area under the curve (AUC) for this model was 0.96.

For the cortical thickness model, we selected the left anterior prefrontal cortex (aPFC) and right retrosplenial cortex (RSC) clusters, which were the largest clusters showing negative and positive effects, respectively, to avoid complete separation in the logistic regression model. LASSO logistic regression retained both clusters. In the final Firth model, reduced left aPFC thickness (beta = −1.81; OR = 0.16, 95% CI = 0.03–0.48; p < 0.001) and greater right RSC thickness (beta = 1.52; OR = 4.58, 95% CI = 1.54–27.33; p = 0.004) were associated with higher odds of aphantasia. The area under the curve (AUC) for the cortical thickness model was 0.93. In addition, we examined the single-variable effect of the left parahippocampal gyrus/entorhinal cortex (PHG/EC) cluster, which showed the largest effect size. Greater left PHG/EC thickness contributed to group discrimination (beta = 2.99; OR = 19.90, 95% CI = 4.27–313.68; p < 0.001). The AUC for this single-variable model was 0.95.

For the graph-theoretical metrics model, given concerns that including all candidate predictors would result in an overly complex model relative to the sample size, we excluded the participation coefficient in the right dorsomedial prefrontal cortex (dmPFC, region 3) and the somatomotor cortex before applying LASSO, based on overlap among regions and their relatively lower theoretical relevance to aphantasia. LASSO regression retained four predictors spanning three network measures. In the final Firth model, a lower clustering coefficient in the left insula (β = −2.41; OR = 0.09, 95% CI = 0.001–0.47; p = 0.002), a lower clustering coefficient in the left prefrontal cortex (β = −0.89; OR = 0.41, 95% CI = 0.007–2.17; p = 0.336), and lower node strength in the left frontal eye field (FEF) (β = −1.32; OR = 0.27, 95% CI = 0.029–0.84; p = 0.022) were associated with higher odds of aphantasia. A higher participation coefficient in the right dmPFC was also associated with higher odds of aphantasia (β = 1.81; OR = 6.14, 95% CI = 1.29–216.11; p = 0.021), consistent with the corresponding univariate result. The area under the curve (AUC) for the graph-theoretical metrics model was 0.99.

Acknowledgements

We thank Dounia Hajhajate, Hanna Kavaliova, and Diane Lamarle for their help in collecting part of the data, Minye Zhan, Elena Grosso, and Benoît Béranger for their suggestions regarding the data analysis and Michel Thiebaut de Schotten for commenting on an early version of our results. The work of Jianghao Liu is supported by specific funding from Dassault Systèmes. The work of Yusaku Takamura is supported by JSPS KAKENHI Grants JP24KK0296 and JST-CRESTJPMJCR23P1. The work of Paolo Bartolomeo is supported by the Agence Nationale de la Recherche through ANR-16-CE37-0005 and ANR-10-IAIHU-06, by the Fondation pour la Recherche sur les AVC through FR-AVC-017, and by the Paris Brain Institute grant ViBER - Vision Beyond External Reality.

Additional information

Contributions

Jianghao Liu: Conceptualization, Data curation, Formal analysis, Funding acquisition, Investigation, Methodology, Project administration, Supervision, Visualization, Writing – original draft, Writing – review & editing; **Yusaku Takamura**: Conceptualization, Data curation, Formal analysis, Methodology, Software, Visualization, Writing – original draft, Writing – review & editing; **Romain Delsanti**: Data curation, Writing – review & editing; **Laurent Cohen:** Resources, Writing – review & editing; **Paolo Bartolomeo:** Conceptualization, Funding acquisition, Project administration, Resources, Supervision, Writing – review & editing.

Materials & correspondence

Requests for materials and correspondence should be addressed to the lead contact Jianghao Liu (*jianghaolouisliu@gmail.com*).

Funding

Funder	Grant reference number	Author
Dassault Systèmes La Fondation (Dassault Foundation)		Jianghao Liu
MEXT | Japan Science and Technology Agency (JST)	https://doi.org/10.52926/jpmjcr23p1	Yusaku Takamura
Agence Nationale de la Recherche (ANR)	ANR-16-CE37-0005	Paolo Bartolomeo
Agence Nationale de la Recherche (ANR)	ANR-10-IAIHU-06	Paolo Bartolomeo

Author ORCID iDs

Yusaku Takamura: https://orcid.org/0009-0009-3891-5605
Laurent Cohen: https://orcid.org/0000-0002-5010-9085
Paolo Bartolomeo: https://orcid.org/0000-0002-2640-6426
Jianghao Liu: https://orcid.org/0000-0001-5732-6827

References

Arcangeli M, Bartolomeo P (2025) The aphantasia paradox: A Sartrean update. *Brain* **148**:3023-3025 https://doi.org/10.1093/brain/awaf233 | PubMed

Bartolomeo P, Liu J, Spagna A (2026) The Fusiform Imagery Node: Where vision meets concepts in the left temporal lobe. *Neuropsychologia* **224**:109398 https://doi.org/10.1016/j.neuropsychologia.2026.109398 | PubMed

Bergmann J, Genç E, Kohler A, Singer W, Pearson J (2016a) Neural Anatomy of Primary Visual Cortex Limits Visual Working Memory. *Cerebral Cortex* **26**:43-50 https://doi.org/10.1093/cercor/bhu168 | PubMed

Bergmann J, Genç E, Kohler A, Singer W, Pearson J (2016b) Smaller Primary Visual Cortex Is Associated with Stronger, but Less Precise Mental Imagery. *Cerebral Cortex* **26**:3838-3850 https://doi.org/10.1093/cercor/bhv186 | PubMed

Bouyer LN, Schwarzkopf DS, Saurels BW, Arnold DH (2025) Objective priming from pre-imagining inputs before binocular rivalry presentations does not predict individual differences in the subjective intensity of imagined experiences. *Cognition* **256**:106048 https://doi.org/10.1016/j.cognition.2024.106048 | PubMed

Cabbai G, Racey C, Simner J, Dance C, Ward J, Forster S (2024) Sensory representations in primary visual cortex are not sufficient for subjective imagery. *Current Biology* **34**:5073-5082.e5. https://doi.org/10.1016/j.cub.2024.09.062 | PubMed

Chang S, Zhang X, Cao Y, Pearson J, Meng M (2025) Imageless imagery in aphantasia revealed by early visual cortex decoding. *Current Biology* **35**:591-599.e4. https://doi.org/10.1016/j.cub.2024.12.012 | PubMed

Cieslak M, Cook PA, He X, Yeh F.-C, Dhollander T, Adebimpe A, Aguirre GK, Bassett DS, Betzel RF, Bourque J, *et al.* (2021) QSIPrep: An integrative platform for preprocessing and reconstructing diffusion MRI data. *Nature Methods* **18**:775-778 https://doi.org/10.1038/s41592-021-01185-5 | PubMed

Coad BM, Postans M, Hodgetts CJ, Muhlert N, Graham KS, Lawrence AD (2020) Structural connections support emotional connections: Uncinate Fasciculus microstructure is related to the ability to decode facial emotion expressions. *Neuropsychologia* **145**:106562 https://doi.org/10.1016/j.neuropsychologia.2017.11.006 | PubMed

Corbetta M, Shulman GL (2002) Control of goal-directed and stimulus-driven attention in the brain. *Nature Reviews Neuroscience* **3** https://doi.org/10.1038/nrn755 | PubMed

Dance CJ, Hole G, Simner J (2023) The role of visual imagery in face recognition and the construction of facial composites. Evidence from Aphantasia. *Cortex* **167**:318-334 https://doi.org/10.1016/j.cortex.2023.06.015 | PubMed

Dance CJ, Jaquiery M, Eagleman DM, Porteous D, Zeman A, Simner J (2021) What is the relationship between Aphantasia, Synaesthesia and Autism?. *Consciousness and Cognition* **89**:103087 https://doi.org/10.1016/j.concog.2021.103087 | PubMed

Dawes AJ, Keogh R, Robuck S, Pearson J (2022) Memories with a blind mind: Remembering the past and imagining the future with aphantasia. *Cognition* **227**:105192 https://doi.org/10.1016/j.cognition.2022.105192 | PubMed

de Reus MA, van den Heuvel MP (2013) The parcellation-based connectome: Limitations and extensions. *NeuroImage* **80**:397-404 https://doi.org/10.1016/j.neuroimage.2013.03.053 | PubMed

Firth D (1993) Bias reduction of maximum likelihood estimates. *Biometrika* **80**:27-38 https://doi.org/10.1093/biomet/80.1.27

Gaser C, Dahnke R, Thompson PM, Kurth F, Luders E, the Alzheimer's Disease Neuroimaging Initiative (2024) CAT: A computational anatomy toolbox for the analysis of structural MRI data. *GigaScience* **13**:giae049 https://doi.org/10.1093/gigascience/giae049 | PubMed

Guevara M, Guevara P, Román C, Mangin J.-F (2020) Superficial white matter: A review on the dMRI analysis methods and applications. *NeuroImage* **212**:116673 https://doi.org/10.1016/j.neuroimage.2020.116673 | PubMed

Huang Z, Tarnal V, Vlisides PE, Janke EL, McKinney AM, Picton P, Mashour GA, Hudetz AG (2021) Anterior insula regulates brain network transitions that gate conscious access. *Cell Reports* **35** https://doi.org/10.1016/j.celrep.2021.109081 | PubMed

Kennis M, van Rooij SJH, Tromp DPM, Fox AS, Rademaker AR, Kahn RS, Kalin NH, Geuze E (2015) Treatment Outcome-Related White Matter Differences in Veterans with Posttraumatic Stress Disorder. *Neuropsychopharmacology* **40**:2434-2442 https://doi.org/10.1038/npp.2015.94 | PubMed

Keogh R, Pearson J (2018) The blind mind: No sensory visual imagery in aphantasia. *Cortex* **105**:53-60 https://doi.org/10.1016/j.cortex.2017.10.012 | PubMed

Keogh R, Wicken M, Pearson J (2023) Fewer intrusive memories in aphantasia: Using the trauma film paradigm as a laboratory model of PTSD. *PsyArXiv* https://doi.org/10.31234/osf.io/7zqfe

Keysers C, Gazzola V, Wagenmakers E.-J (2020) Using Bayes factor hypothesis testing in neuroscience to establish evidence of absence. *Nature Neuroscience* **23**:788-799 https://doi.org/10.1038/s41593-020-0660-4 | PubMed

Kruper J, Yeatman JD, Richie-Halford A, Bloom D, Grotheer M, Caffarra S, Kiar G, Karipidis II, Roy E, Chandio BQ, *et al.* (2021) Evaluating the Reliability of Human Brain White Matter Tractometry. *Aperture Neuro* **1** https://doi.org/10.52294/e6198273-b8e3-4b63-babb-6e6b0da10669 | PubMed

Larivière S, Bayrak Ş, Vos de Wael R, Benkarim O, Herholz P, Rodriguez-Cruces R, Paquola C, Hong SJ, Misic B, Evans AC, *et al.* (2023) BrainStat: A toolbox for brain-wide statistics and multimodal feature associations. *NeuroImage* **266**:119807 https://doi.org/10.1016/j.neuroimage.2022.119807 | PubMed

Liu J (2026) A neural model of conscious mental imagery and aphantasia. *Neuropsychologia* **224**:109392 https://doi.org/10.1016/j.neuropsychologia.2026.109392 | PubMed

Liu J (2026) Aphantasia as a window into unconscious internal processing. *PsyArXiv* https://doi.org/10.31234/osf.io/rc9y7_v1

Liu J, Bartolomeo P (2023) Probing the unimaginable: The impact of aphantasia on distinct domains of visual mental imagery and visual perception. *Cortex* **166**:338-347 https://doi.org/10.1016/j.cortex.2023.06.003 | PubMed

Liu J, Bartolomeo P (2025) Aphantasia as a functional disconnection. *Trends in Cognitive Sciences* **29**:963-964 https://doi.org/10.1016/j.tics.2025.05.012 | PubMed

Liu J, Cohen L, Pallier C, Dehaene S, Zhan M, Bartolomeo P (2025a) Face-, color-, and word-specific patches in the human orbitofrontal cortex. *bioRxiv* https://doi.org/10.1101/2025.04.22.650059

Liu J, Zhan M, Hajhajate D, Spagna A, Dehaene S, Cohen L, Bartolomeo P (2025b) Visual mental imagery in typical imagers and in aphantasia: A millimeter-scale 7-T fMRI study. *Cortex* **185**:113-132 https://doi.org/10.1016/j.cortex.2025.01.013 | PubMed

Marks DF (1973) Visual Imagery Differences in the Recall of Pictures. *British Journal of Psychology* **64**:17-24 https://doi.org/10.1111/j.2044-8295.1973.tb01322.x | PubMed

Mary A, Dayan J, Leone G, Postel C, Fraisse F, Malle C, Vallée T, Klein-Peschanski C, Viader F, de la Sayette V, *et al.* (2020) Resilience after trauma: The role of memory suppression. *Science* **367**:eaay8477 https://doi.org/10.1126/science.aay8477 | PubMed

Mawtus B, Renwick F, Thomas BR, Reeder RR (2024) The Impact of Aphantasia on Mental Healthcare Experiences. *Collabra: Psychology* **10**:127416 https://doi.org/10.1525/collabra.127416

Meisler SL, Kubota E, Grotheer M, Gabrieli JDE, Grill-Spector K (2024) A practical guide for combining functional regions of interest and white matter bundles. *Frontiers in Neuroscience* **18** https://doi.org/10.3389/fnins.2024.1385847 | PubMed

Milton F, Fulford J, Dance C, Gaddum J, Heuerman-Williamson B, Jones K, Knight KF, MacKisack M, Winlove C, Zeman A (2021) Behavioral and Neural Signatures of Visual Imagery Vividness Extremes: Aphantasia versus Hyperphantasia. *Cerebral Cortex Communications* **2**:tgab035 https://doi.org/10.1093/texcom/tgab035 | PubMed

Montabes De La Cruz BM, Abbatecola C, Luciani RS, Paton AT, Bergmann J, Vetter P, Petro LS, Muckli LF (2024) Decoding sound content in the early visual cortex of aphantasic participants. *Current Biology* **34**:5083-5089.e3. https://doi.org/10.1016/j.cub.2024.09.008 | PubMed

Monzel M, Karneboge J, Reuter M (2024a) Affective processing in aphantasia and potential overlaps with alexithymia: Mental imagery facilitates the recognition of emotions in oneself and others. *Biomarkers in Neuropsychiatry* **11**:100106 https://doi.org/10.1016/j.bionps.2024.100106

Monzel M, Leelaarporn P, Lutz T, Schultz J, Brunheim S, Reuter M, McCormick C (2024b) Hippocampal-occipital connectivity reflects autobiographical memory deficits in aphantasia. *eLife* **13** https://doi.org/10.7554/eLife.94916.2

Moser EI, Roudi Y, Witter MP, Kentros C, Bonhoeffer T, Moser M.-B (2014) Grid cells and cortical representation. *Nature Reviews Neuroscience* **15**:466-481 https://doi.org/10.1038/nrn3766 | PubMed

Noble C, Taylor NL, Milton F, Fulford J, Tan JB, O'Callaghan C, Zeman A, Shine JM (2026) Seeing through the static: Reduced imagery vividness in aphantasia is associated with impaired temporal lobe signal complexity. *Neuropsychologia* **221**:109322 https://doi.org/10.1016/j.neuropsychologia.2025.109322 | PubMed

Nobre AC, Gresch D (2025) How the brain shifts between external and internal attention. *Neuron* **113**:2382-2398 https://doi.org/10.1016/j.neuron.2025.06.013 | PubMed

Parlatini V, Itahashi T, Lee Y, Liu S, Nguyen TT, Aoki YY, Forkel SJ, Catani M, Rubia K, Zhou JH, *et al.* (2023) White matter alterations in Attention-Deficit/Hyperactivity Disorder (ADHD): A systematic review of 129 diffusion imaging studies with meta-analysis. *Molecular Psychiatry* **28**:4098-4123 https://doi.org/10.1038/s41380-023-02173-1 | PubMed

Pounder Z, Jacob J, Evans S, Loveday C, Eardley AF, Silvanto J (2022) Only minimal differences between individuals with congenital aphantasia and those with typical imagery on neuropsychological tasks that involve imagery. *Cortex* **148**:180-192 https://doi.org/10.1016/j.cortex.2021.12.010 | PubMed

Ren J, An N, Lin C, Zhang Y, Sun Z, Zhang W, Li S, Guo N, Cui W, Hu Q, *et al.* (2025) DeepPrep: An accelerated, scalable and robust pipeline for neuroimaging preprocessing empowered by deep learning. *Nature Methods* **22**:473-476 https://doi.org/10.1038/s41592-025-02599-1 | PubMed

Rubinov M, Sporns O (2010) Complex network measures of brain connectivity: Uses and interpretations. *NeuroImage*. *Computational Models of the Brain* **52**:1059-1069 https://doi.org/10.1016/j.neuroimage.2009.10.003 | PubMed

Sasikumar S, Strafella AP (2021) The neuroimaging evidence of brain abnormalities in functional movement disorders. *Brain* **144**:2278-2283 https://doi.org/10.1093/brain/awab131 | PubMed

Schaefer A, Kong R, Gordon EM, Laumann TO, Zuo X.-N, Holmes AJ, Eickhoff SB, Yeo BTT (2018) Local-Global Parcellation of the Human Cerebral Cortex from Intrinsic Functional Connectivity MRI. *Cerebral Cortex* **28**:3095-3114 https://doi.org/10.1093/cercor/bhx179 | PubMed

Scholz CO, Monzel M, Kvamme TL, Liu J, Silvanto J (2026) An integration model of mental imagery and aphantasia: Conceptual framework, neuromechanistic pathways, and clinical implications. *Neuropsychologia* **225**:109401 https://doi.org/10.1016/j.neuropsychologia.2026.109401 | PubMed

Scholz CO, Monzel M, Liu J (2025) Absence of shared representation in the visual cortex challenges unconscious imagery in aphantasia. *Current Biology* **35**:R645-R646 https://doi.org/10.1016/j.cub.2025.05.009 | PubMed

Siena MJ, Simons JS (2024) Metacognitive Awareness and the Subjective Experience of Remembering in Aphantasia. *Journal of Cognitive Neuroscience* **36**:1578-1598 https://doi.org/10.1162/jocn_a_02120 | PubMed

Sokolowski HM, Levine B (2023) Common neural substrates of diverse neurodevelopmental disorders. *Brain* **146**:438-447 https://doi.org/10.1093/brain/awac387 | PubMed

Song S.-K, Sun S.-W, Ramsbottom MJ, Chang C, Russell J, Cross AH (2002) Dysmyelination Revealed through MRI as Increased Radial (but Unchanged Axial) Diffusion of Water. *NeuroImage* **17**:1429-1436 https://doi.org/10.1006/nimg.2002.1267 | PubMed

Sotiropoulos SN, Zalesky A (2019) Building connectomes using diffusion MRI: Why, how and but. *NMR in Biomedicine* **32**:e3752 https://doi.org/10.1002/nbm.3752 | PubMed

Spagna A, Hajhajate D, Liu J, Bartolomeo P (2021) Visual mental imagery engages the left fusiform gyrus, but not the early visual cortex: A meta-analysis of neuroimaging evidence. *Neuroscience & Biobehavioral Reviews* **122**:201-217 https://doi.org/10.1016/j.neubiorev.2020.12.029 | PubMed

Suggate SP, Milton F, Tree J (2026) Multimodal mental comparisons in those with and without aphantasia. *Neuropsychologia* **222**:109373 https://doi.org/10.1016/j.neuropsychologia.2026.109373 | PubMed

Thiebaut de Schotten M, Dell'Acqua F, Forkel SJ, Simmons A, Vergani F, Murphy DG, Catani M (2011) A lateralized brain network for visuospatial attention. *Nat Neurosci* **14**:1245-1246 https://doi.org/10.1038/nn.2905 | PubMed

Thomas C, Avidan G, Humphreys K, Jung K, Gao F, Behrmann M (2009) Reduced structural connectivity in ventral visual cortex in congenital prosopagnosia. *Nature Neuroscience* **12**:29-31 https://doi.org/10.1038/nn.2224 | PubMed

Thomas C, Avram A, Pierpaoli C, Baker C (2015) Diffusion MRI properties of the human uncinate fasciculus correlate with the ability to learn visual associations. *Cortex: A Journal Devoted to the Study of the Nervous System and Behavior* **72**:65-78 https://doi.org/10.1016/j.cortex.2015.01.023 | PubMed

Travers BG, Adluru N, Ennis C, Tromp DPM, Destiche D, Doran S, Bigler ED, Lange N, Lainhart JE, Alexander AL (2012) Diffusion Tensor Imaging in Autism Spectrum Disorder: A Review. *Autism Research* **5**:289-313 https://doi.org/10.1002/aur.1243 | PubMed

Treisman A (2007) How the deployment of attention determines what we see. In: *Progress in Psychological Science around the World. Volume 1 Neural, Cognitive and Developmental Issues* Psychology Press. https://doi.org/10.1080/13506280500195250 | PubMed

Vann SD, Aggleton JP, Maguire EA (2009) What does the retrosplenial cortex do?. *Nature Reviews Neuroscience* **10**:792-802 https://doi.org/10.1038/nrn2733 | PubMed

Warrington S, Bryant KL, Khrapitchev AA, Sallet J, Charquero-Ballester M, Douaud G, Jbabdi S, Mars RB, Sotiropoulos SN (2020) XTRACT - Standardised protocols for automated tractography in the human and macaque brain. *NeuroImage* **217**:116923 https://doi.org/10.1016/j.neuroimage.2020.116923 | PubMed

Zeman A (2024) Aphantasia and hyperphantasia: Exploring imagery vividness extremes. *Trends in Cognitive Sciences* **28**:467-480 https://doi.org/10.1016/j.tics.2024.02.007 | PubMed

Zeman A, Milton F, Della Sala S, Dewar M, Frayling T, Gaddum J, Hattersley A, Heuerman-Williamson B, Jones K, MacKisack M (2020) Phantasia–the psychological significance of lifelong visual imagery vividness extremes. *Cortex* **130**:426-440 https://doi.org/10.1016/j.cortex.2020.04.003 | PubMed

Zhang H, Schneider T, Wheeler-Kingshott CA, Alexander DC (2012) NODDI: Practical *in vivo* neurite orientation dispersion and density imaging of the human brain. *NeuroImage* **61**:1000-1016 https://doi.org/10.1016/j.neuroimage.2012.03.072 | PubMed

Peer reviews

Reviewer #1 (Public review):

Summary

In this paper, the authors provide a systematic investigation of structural brain differences associated with congenital aphantasia (self-reported lifelong absence of voluntary visual imagery). Specifically, the authors analysed a structural neuroimaging dataset involving 18 individuals with aphantasia and 18 visualizers to test two competing hypotheses: (1) that aphantasia reflects alterations in visual pathways and early visual cortex, and (2) that it instead reflects differences in higher-order frontotemporal and cingulate systems. To test these hypotheses, the authors employed multiple analysis approaches (e.g., cortical morphometry, tractometry, graph-theoretic network analysis).

They report structural differences between the two groups in frontotemporal and cingulate systems. In contrast, they found no reliable group differences in early visual cortex or major visual tracts. On this basis, they propose that aphantasia is primarily associated with differences in higher-order systems supporting integration and conscious access to internally generated representations, rather than with deficits in sensory visual representations themselves.

Strengths

(1) The present work addresses an important gap in the mental imagery literature, providing a systematic investigation of structural neuroimaging differences in congenital aphantasia. By showing that structural differences between aphantasics and visualizers are mainly concentrated in frontotemporal and cingulate systems (rather than in visual cortex), it makes an important step toward a better understanding of individual differences in mental imagery and provides a set of candidate regions for future mechanistic work.

(2) A key strength of the study is the multimodal approach employed to address the main research question, integrating tractometry, functional region-of-interest (fROI)-based

tractography, graph-theoretic network analysis, and surface-based cortical morphometry, which provide a converging assessment of structural differences between aphantasics and visualizers.

(3) The complementary use of Bayesian analyses alongside NHST to assess evidence for null results is a further strength of this work.

Weaknesses:

(1) A weakness of this work is related to aspects of the framing and, in particular, what can be confidently inferred from the results. The framing of existing accounts of aphantasia in the Introduction appears limited in that it reduces the views on aphantasia to two options (sensory strength account versus conscious access account) without acknowledging a third distinct position, namely that aphantasia reflects a specific deficit in the voluntary generation of imagery (Milton et al., 2021; Zeman et al., 2015, 2020; Whiteley, 2021; Cavedon-Taylor, 2022). Like the conscious access account, the view that aphantasia involves a deficit in the generation of sensory representation also speaks against the hypothesis of reduced sensory strength of internally generated representations. This third view could be acknowledged/discussed as it also maps quite well onto the presented results.

(2) Relatedly, I think the main weakness of the paper concerns the interpretation of results being restricted to a lack of "conscious access". The paper frames its findings as mainly evidence for a conscious access failure, the view that visual representations are generated by aphantasics but cannot be consciously accessed. However, the structural findings are equally consistent with a voluntary generation failure, especially since the same higher-order regions examined can also be implicated in the top-down generation and control of imagery. The authors themselves initially define aphantasia as "lifelong absence of voluntary visual imagery". Given the nature of structural imaging data (as opposed to functional data), it is not possible with the present study to distinguish between a lack of generation versus a lack of conscious access. As such, examining this alternative interpretation appears appropriate, and it would considerably strengthen the paper. Structural MRI alone is not sufficient to dissociate imagery generation from conscious access, as these are fundamentally functional questions.

(3) Some inconsistency and lack of clarity around the specific choice of regions/networks, which could be better motivated and explained. E.g., the "core imagery network" analysed in the white-matter connections analysis was derived from a previous 7T study (with which the sample partially overlaps) and is not necessarily the network most commonly associated with visual imagery in the literature (e.g., see Dijkstra et al., 2019; Pearson, 2019). It is, for instance, unclear why V1 was examined in the cortical thickness analysis but not in the previous one, given that both analyses are related to the visual pathway hypothesis. Related to this, in the graph-theoretic analysis, the rationale for network selection is inconsistently established in the Introduction. The attention and salience networks do have some grounding in the Introduction through the mention of specific regions such as FEF and anterior insula, though these are discussed as individual regions rather than as networks. However, the default mode network receives no motivation in the Introduction. More explicit elaboration on these choices would be appropriate.

(3) The interpretation provided in the Discussion tends to oversimplify what is in fact a heterogeneous and rich set of structural findings into a relatively coherent mechanistic account. The observed differences are spatially and directionally variable across tracts, cortical regions, and metrics: e.g., FA is reduced in the UF and posterior interparietal corpus callosum but increased in the dorsal cingulum; cortical thickness is reduced in aPFC but increased in medial temporal regions, and so forth. The Discussion acknowledges this in part (e.g., proposing increased dorsal cingulum FA as potentially compensatory) but does not address the directional heterogeneity systematically. The authors could discuss more

explicitly what the opposing directions of effects mean for their overall interpretation. Relatedly, some parts of the Discussion link specific structural findings to specific imagery processes in ways that go beyond what the current data can support. The authors could more clearly distinguish between what the structural data show and what functional interpretations are taken from prior work.

https://doi.org/10.7554/eLife.111728.1.sa3

Reviewer #2 (Public review):

Summary:

This paper addresses whether congenital aphantasia reflects an alteration of visual representations themselves, or rather of the systems that allow internally generated representations to reach conscious experience.

Strengths:

The study is novel and ambitious. The authors combine several complementary structural MRI approaches in a rare and well-characterised population, and the convergence of the findings toward frontotemporal and cingulate systems, with relative sparing of early visual cortex and major visual pathways, is particularly interesting because it could affect the way visual imagery is modelled and tested experimentally and clinically.

Weaknesses:

Overall, I found the manuscript conceptually and methodologically strong. My main concern regards the interpretation of the anatomical findings, rather than the findings per se. The authors discuss their results within a rich cognitive framework. However, the current dataset does not appear to include independent behavioural or neuropsychological measures that would allow the proposed cognitive interpretation to be tested in the same participants. As a result, the manuscript sometimes moves quite rapidly from 'these structural differences involve systems associated with higher-order control, salience, conscious access' to 'these structural differences may explain the cognitive mechanisms of aphantasia'. I agree that this is the most interesting interpretation, and probably the right one to explore. Although plausible, it remains indirect. The authors already acknowledge this point when discussing memory, affective control, and semantic processing. However, the same logic should be extended to the interpretation of the full set of findings. For example, if the salience/anterior insula findings are interpreted in relation to access to internally generated representations, it would be useful to know whether aphantasic participants also differ behaviourally on tasks tapping interoception or related aspects of internal monitoring. I appreciate that collecting additional behavioural data may not be feasible at this stage, especially given the difficulty of recruiting participants with such a specific manifestation. However, I think it should be acknowledged more explicitly in a dedicated limitation paragraph.

https://doi.org/10.7554/eLife.111728.1.sa2

Reviewer #3 (Public review):

Summary:

The authors investigate the structural brain basis of congenital aphantasia, a condition characterised by a lifelong absence of voluntary mental imagery. They test two competing accounts: one predicting structural differences in early visual pathways, the other predicting differences in higher-order frontotemporal and cingulate systems. To do this, they combine four complementary structural imaging approaches: white-matter microstructure profiling

along anatomically defined tracts, tractography seeded from functional regions of interest, whole-brain structural network analysis, and cortical thickness mapping. The main finding is that white-matter differences are selective for frontotemporal and cingulate pathways and absent in early visual pathways, which the authors interpret as support for the higher-order account.

Strengths:

The multi-modal design is a genuine strength: running four independent analyses increases the chance of detecting real effects and of identifying false positives that appear in only one stream. The statistical choices within each analysis are appropriate. Permutation-based correction with a threshold-free method is well-suited to the tract-level comparisons. The use of Bayes factors to quantify evidence for null results, rather than simply reporting non-significant tests, is particularly valuable here, since the absence of visual pathway differences is central to the argument. The robustness checks across multiple brain parcellations for the network analysis strengthen confidence in those findings.

Weaknesses:

The main limitation concerns the relationship between two of the analysis streams. The measure used to weight structural connections in the network analysis is calibrated to match fiber density estimates derived from the same diffusion signal that drives the white-matter microstructure differences. If the two groups differ in tissue organisation in certain pathways (which the microstructure analysis suggests they do), that difference will feed into both measures. The authors should acknowledge this dependency when discussing convergence across analyses.

More broadly, the imaging metrics used throughout (measures of fiber organisation and weighted connection counts) reflect what the diffusion model captures from the tissue and cannot be directly read as measures of axon number or connection strength. This is a known limitation of the field, but it is relevant to the strength of structural claims made in this paper.

The network analysis is presented without comparison to a null network. Without this, it is hard to know whether the node-level differences reflect specific network topology or simply follow from overall differences in connectivity weight or density between groups.

The study runs four separate discovery analyses on the same 36 participants, each corrected within itself but with no control across analysis streams. At 18 participants per group, this is exploratory work. Some of the language used in the abstract and discussion, like "first comprehensive characterization" and "selective structural phenotype", reads as more definitive than the data support at this sample size. Framing the results as hypotheses to be replicated would make the paper stronger.

The paper frames the results as distinguishing between two competing accounts. The positive evidence for the higher-order account is clear. The absence of differences in visual pathways is a different kind of result: it means such differences were not detected in this sample, not that visual pathways are uninvolved. The discussion at times moves toward that stronger conclusion, which the data do not support.

The cortical thickness analysis finds one cluster in the predicted direction, while the other analyses each return multiple effects. One cluster in a whole-brain search with 18 participants per group is not strong evidence and should not be presented as equivalent to the other results.

Effect sizes are reported without confidence intervals throughout. With 18 participants per group, the uncertainty around those estimates is large, and confidence intervals would give readers a more accurate sense of what can be concluded.

https://doi.org/10.7554/eLife.111728.1.sa1

Author response:

Reviewer #1 (Public review):

Summary:

In this paper, the authors provide a systematic investigation of structural brain differences associated with congenital aphantasia (self-reported lifelong absence of voluntary visual imagery). Specifically, the authors analysed a structural neuroimaging dataset involving 18 individuals with aphantasia and 18 visualizers to test two competing hypotheses: (1) that aphantasia reflects alterations in visual pathways and early visual cortex, and (2) that it instead reflects differences in higher-order frontotemporal and cingulate systems. To test these hypotheses, the authors employed multiple analysis approaches (e.g., cortical morphometry, tractometry, graph-theoretic network analysis).

They report structural differences between the two groups in frontotemporal and cingulate systems. In contrast, they found no reliable group differences in early visual cortex or major visual tracts. On this basis, they propose that aphantasia is primarily associated with differences in higher-order systems supporting integration and conscious access to internally generated representations, rather than with deficits in sensory visual representations themselves.

Strengths:

(1) The present work addresses an important gap in the mental imagery literature, providing a systematic investigation of structural neuroimaging differences in congenital aphantasia. By showing that structural differences between aphantasics and visualizers are mainly concentrated in frontotemporal and cingulate systems (rather than in visual cortex), it makes an important step toward a better understanding of individual differences in mental imagery and provides a set of candidate regions for future mechanistic work.

(2) A key strength of the study is the multimodal approach employed to address the main research question, integrating tractometry, functional region-of-interest (fROI)-based tractography, graph-theoretic network analysis, and surface-based cortical morphometry, which provide a converging assessment of structural differences between aphantasics and visualizers.

(3) The complementary use of Bayesian analyses alongside NHST to assess evidence for null results is a further strength of this work.

Weaknesses:

(1) A weakness of this work is related to aspects of the framing and, in particular, what can be confidently inferred from the results. The framing of existing accounts of aphantasia in the Introduction appears limited in that it reduces the views on aphantasia to two options (sensory strength account versus conscious access account) without acknowledging a third distinct position, namely that aphantasia reflects a specific deficit in the voluntary generation of imagery (Milton et al., 2021; Zeman et al., 2015, 2020; Whiteley, 2021; Cavedon-Taylor, 2022). Like the conscious access account, the view that aphantasia involves a deficit in the generation of sensory representation also speaks against the hypothesis of reduced sensory strength of internally generated representations. This third view could be acknowledged/discussed as it also maps quite well onto the presented results.

> *(2) Relatedly, I think the main weakness of the paper concerns the interpretation of results being restricted to a lack of "conscious access". The paper frames its findings as mainly evidence for a conscious access failure, the view that visual representations are generated by aphantasics but cannot be consciously accessed. However, the structural findings are equally consistent with a voluntary generation failure, especially since the same higher-order regions examined can also be implicated in the top-down generation and control of imagery. The authors themselves initially define aphantasia as "lifelong absence of voluntary visual imagery". Given the nature of structural imaging data (as opposed to functional data), it is not possible with the present study to distinguish between a lack of generation versus a lack of conscious access. As such, examining this alternative interpretation appears appropriate, and it would considerably strengthen the paper. Structural MRI alone is not sufficient to dissociate imagery generation from conscious access, as these are fundamentally functional questions.*
>
> *(3) Some inconsistency and lack of clarity around the specific choice of regions/networks, which could be better motivated and explained. E.g., the "core imagery network" analysed in the white-matter connections analysis was derived from a previous 7T study (with which the sample partially overlaps) and is not necessarily the network most commonly associated with visual imagery in the literature (e.g., see Dijkstra et al., 2019; Pearson, 2019). It is, for instance, unclear why V1 was examined in the cortical thickness analysis but not in the previous one, given that both analyses are related to the visual pathway hypothesis. Related to this, in the graph-theoretic analysis, the rationale for network selection is inconsistently established in the Introduction. The attention and salience networks do have some grounding in the Introduction through the mention of specific regions such as FEF and anterior insula, though these are discussed as individual regions rather than as networks. However, the default mode network receives no motivation in the Introduction. More explicit elaboration on these choices would be appropriate.*
>
> *(4) The interpretation provided in the Discussion tends to oversimplify what is in fact a heterogeneous and rich set of structural findings into a relatively coherent mechanistic account. The observed differences are spatially and directionally variable across tracts, cortical regions, and metrics: e.g., FA is reduced in the UF and posterior interparietal corpus callosum but increased in the dorsal cingulum; cortical thickness is reduced in aPFC but increased in medial temporal regions, and so forth. The Discussion acknowledges this in part (e.g., proposing increased dorsal cingulum FA as potentially compensatory) but does not address the directional heterogeneity systematically. The authors could discuss more explicitly what the opposing directions of effects mean for their overall interpretation. Relatedly, some parts of the Discussion link specific structural findings to specific imagery processes in ways that go beyond what the current data can support. The authors could more clearly distinguish between what the structural data show and what functional interpretations are taken from prior work.*

We will add two recent in-press Cortex papers to the Discussion. One provides lesion-based double-dissociation evidence against V1 as a necessary causal substrate of visual imagery. The other shows that aphantasic individuals can display visualizer-like oculomotor patterns during mental map exploration despite reporting little or no imagery vividness. Together, these studies help clarify our interpretation of our null V1 findings and structural effects in higher-order brain regions, which are consistent with aphantasia involving altered integration or access rather than a primary V1-dependent imagery deficit.

> ***Reviewer #2 (Public review):***
>
> *Summary:*

> *This paper addresses whether congenital aphantasia reflects an alteration of visual representations themselves, or rather of the systems that allow internally generated representations to reach conscious experience.*
>
> *Strengths:*
>
> *The study is novel and ambitious. The authors combine several complementary structural MRI approaches in a rare and well-characterised population, and the convergence of the findings toward frontotemporal and cingulate systems, with relative sparing of early visual cortex and major visual pathways, is particularly interesting because it could affect the way visual imagery is modelled and tested experimentally and clinically.*
>
> *Weaknesses:*
>
> *Overall, I found the manuscript conceptually and methodologically strong. My main concern regards the interpretation of the anatomical findings, rather than the findings per se. The authors discuss their results within a rich cognitive framework. However, the current dataset does not appear to include independent behavioural or neuropsychological measures that would allow the proposed cognitive interpretation to be tested in the same participants. As a result, the manuscript sometimes moves quite rapidly from 'these structural differences involve systems associated with higher-order control, salience, conscious access' to 'these structural differences may explain the cognitive mechanisms of aphantasia'. I agree that this is the most interesting interpretation, and probably the right one to explore. Although plausible, it remains indirect. The authors already acknowledge this point when discussing memory, affective control, and semantic processing. However, the same logic should be extended to the interpretation of the full set of findings. For example, if the salience/anterior insula findings are interpreted in relation to access to internally generated representations, it would be useful to know whether aphantasic participants also differ behaviourally on tasks tapping interoception or related aspects of internal monitoring. I appreciate that collecting additional behavioural data may not be feasible at this stage, especially given the difficulty of recruiting participants with such a specific manifestation. However, I think it should be acknowledged more explicitly in a dedicated limitation paragraph.*

We thank the reviewer for this thoughtful and constructive comment. Lack of introspective report of voluntary imagery is arguably the defining signature of aphantasia. This motivated us to primarily interpret our anatomical findings in a broader cognitive context of higher-order control, internal monitoring, and conscious access in aphantasia. We expect that a reliable behavioural test measuring imagery sensitivity and accessibility would allow us to direct link these findings to individual imagery ability. Nevertheless, to our best knowledge, this kind of test on imagery is still missing. Instead, our findings point to some plausible structural signature or brain regions that may be related to conscious imagery, which motivate future studies to examine their direct or causal roles. We agree with the reviewer, future studies should test the relationship between these anatomical structures and the accessibility to internal representation, together with related aspects of internal monitoring. We will therefore add a dedicated paragraph to discuss the plausible cognitive mechanisms during the revision.

> ***Reviewer #3 (Public review):***
>
> *Summary:*
>
> *The authors investigate the structural brain basis of congenital aphantasia, a condition characterised by a lifelong absence of voluntary mental imagery. They test two competing accounts: one predicting structural differences in early visual pathways, the other predicting differences in higher-order frontotemporal and cingulate systems. To do*

this, they combine four complementary structural imaging approaches: white-matter microstructure profiling along anatomically defined tracts, tractography seeded from functional regions of interest, whole-brain structural network analysis, and cortical thickness mapping. The main finding is that white-matter differences are selective for frontotemporal and cingulate pathways and absent in early visual pathways, which the authors interpret as support for the higher-order account.

Strengths:

The multi-modal design is a genuine strength: running four independent analyses increases the chance of detecting real effects and of identifying false positives that appear in only one stream. The statistical choices within each analysis are appropriate. Permutation-based correction with a threshold-free method is well-suited to the tract-level comparisons. The use of Bayes factors to quantify evidence for null results, rather than simply reporting non-significant tests, is particularly valuable here, since the absence of visual pathway differences is central to the argument. The robustness checks across multiple brain parcellations for the network analysis strengthen confidence in those findings.

Weaknesses:

The main limitation concerns the relationship between two of the analysis streams. The measure used to weight structural connections in the network analysis is calibrated to match fiber density estimates derived from the same diffusion signal that drives the white-matter microstructure differences. If the two groups differ in tissue organisation in certain pathways (which the microstructure analysis suggests they do), that difference will feed into both measures. The authors should acknowledge this dependency when discussing convergence across analyses.

More broadly, the imaging metrics used throughout (measures of fiber organisation and weighted connection counts) reflect what the diffusion model captures from the tissue and cannot be directly read as measures of axon number or connection strength. This is a known limitation of the field, but it is relevant to the strength of structural claims made in this paper.

The network analysis is presented without comparison to a null network. Without this, it is hard to know whether the node-level differences reflect specific network topology or simply follow from overall differences in connectivity weight or density between groups.

The study runs four separate discovery analyses on the same 36 participants, each corrected within itself but with no control across analysis streams. At 18 participants per group, this is exploratory work. Some of the language used in the abstract and discussion, like "first comprehensive characterization" and "selective structural phenotype", reads as more definitive than the data support at this sample size. Framing the results as hypotheses to be replicated would make the paper stronger.

The paper frames the results as distinguishing between two competing accounts. The positive evidence for the higher-order account is clear. The absence of differences in visual pathways is a different kind of result: it means such differences were not detected in this sample, not that visual pathways are uninvolved. The discussion at times moves toward that stronger conclusion, which the data do not support.

The cortical thickness analysis finds one cluster in the predicted direction, while the other analyses each return multiple effects. One cluster in a whole-brain search with 18 participants per group is not strong evidence and should not be presented as equivalent to the other results.

> *Effect sizes are reported without confidence intervals throughout. With 18 participants per group, the uncertainty around those estimates is large, and confidence intervals would give readers a more accurate sense of what can be concluded.*

We are grateful to the Reviewer for the constructive and thoughtful assessment of our manuscript. In response to the reviewer's comments, we will revise the manuscript to clarify the dependency between diffusion-derived analysis streams, to state more explicitly the biological limits of diffusion MRI metrics, to add a null-network sensitivity analysis for the clustering coefficient findings, to include confidence intervals for reported effect sizes, and to temper the interpretation of the cortical thickness result. We will also revise the Abstract and Discussion to better reflect the exploratory nature of the study and to frame the findings as hypotheses requiring replication in larger independent samples. We believe that these revisions will make the manuscript more balanced, transparent, and appropriately cautious, while preserving the central conclusion that congenital aphantasia is associated with structural differences centered on higher-order frontotemporal and cingulate systems.

https://doi.org/10.7554/eLife.111728.1.sa0